SKB

# TECHNICAL REPORT 91-44

## Fluid and solute transport in a network of channels

Luis Moreno, Ivars Neretnieks

Department of Chemical Engineering,
Royal Institute of Technology, Stockholm
Sweden

September 1991

**SVENSK KÄRNBRÄNSLEHANTERING AB**
*SWEDISH NUCLEAR FUEL AND WASTE MANAGEMENT CO*

BOX 5864 S-102 48 STOCKHOLM

TEL 08-665 28 00 TELEX 13108 SKB S
TELEFAX 08-661 57 19

# FLUID AND SOLUTE TRANSPORT IN A NETWORK OF CHANNELS

Luis Moreno, Ivars Neretnieks

Department of Chemical Engineering,
Royal Institute of Technology, Stockholm, Sweden

September 1991

# FLUID AND SOLUTE TRANSPORT IN A NETWORK OF CHANNELS

Luis Moreno
Ivars Neretnieks

1991-09-04

Department of Chemical Engineering
Royal Institute of Technology
S-100 44 Stockholm, Sweden

KAT 91/08

## ABSTRACT

A three-dimensional channel network model is presented. The fluid flow and solute transport are assumed to take place through a network of connected channels. The channels are generated assuming that the conductances are lognormally distributed. The flow is calculated resolving the pressure distribution and the solute transport is calculated by using a particle tracking technique. The model includes diffusion into the rock matrix and sorption within the matrix in addition to advection along the channel network. Different approaches are used to describe the channel volume and its relation to the conductivity. To quantify the diffusion into the rock matrix the size of the flow wetted surface (contact surface between the channel and the rock) is needed in addition to the diffusion properties and the sorption capacity of the rock.

Two different geometries were simulated: regional parallel flow and convergent flow toward a tunnel. In the generation of the channel network, it is found that its connectivity is reduced when the standard deviation in conductances is increased. For large standard deviations, the water conducting channels are found to be few. Standard deviations for the distribution of the effluent channel flowrates were calculated. Comparisons were made with experimental data from drifts and tunnels as well as boreholes as a means to validate the model.

TABLE OF CONTENTS

## SUMMARY

A new model is proposed to describe flow and transport in fractured rocks. It is based on the concept of a network of channels. This approach is backed by observations in drifts and tunnels that flow in fractured rocks takes place in sparse narrow effluent locations with widths typically less than 10 cm and a channel frequency of one channel per a few square meters to one channel per more than a hundred square meters. Observations in boreholes also indicate that there are large distances, tens to hundreds of meters, between the most conductive sections in boreholes.

For visualization purposes our model is displayed on a rectangular grid. The individual channels are given stochastically selected conductances and volumes. Flowrate calculations have been performed in grids of sizes 20*20*20 channels in most cases but larger grids have also been used. For large standard deviations in conductances, greater than 1.6 in the log normal distribution (base 10), channeling becomes pronounced with most of the water flowing in a few paths. The effluent patterns and flowrate distributions obtained in the simulations have been compared to three different field measurements in drifts and tunnels of flowrate distributions. Standard deviations of channels conductances were found to be between 1.6 and 2.4 or more in some cases. Channel lengths were found to vary between 1.2 m and 10.2 m in the different sites. In one site where detailed borehole measurements were available the channel length could be assessed independently and was found to be 1.7 m as compared to the 1.2 m obtained from the drift inflow measurements.

A particle tracking technique was used to simulate solute transport in the network. Nonsorbing as well as sorbing tracer transport can be simulated and by a special technique also tracers which diffuse into the rock matrix can be simulated.

Tracer measurements in one site, Stripa, were used to compare dispersivities. These were found to be large, Peclet numbers less than 5 both in simulations and the field results. From the Stripa tracer data it was also found that the tracers were taken up into the rock matrix by molecular diffusion. The surface area needed for this uptake was estimated to be between 0.2-20 $m^2/m^3$ for different tracers. The wetted surface for the model estimated from flowrate distribution data indicate a wetted surface of 0.2- 0.4 $m^2/m^3$.

# 1 INTRODUCTION AND BACKGROUND

Flow and solute transport in fractured rock has been found to be poorly described by the advection dispersion concept and equations. Field observations show that there are strong channeling effects and that when it is attempted to evaluate the dispersion coefficient this seemingly increases with distance (Abelin et al., 1987; Neretnieks et al., 1987; Neretnieks, 1991). Field observations in drifts and tunnels also show that flow channels are sparse and that the flowrate distribution is very large among channels (Neretnieks et al., 1987). For short distances it has been proposed that the flow and solute transport might better be described as taking place in a bundle of independent channels (Neretnieks et al., 1987). For longer distances channels have a larger chance to meet and a network concept seems more appropriate. For very long distances it is conceivable that the mixing between channels is large enough for the transport to behave as described by the advection-dispersion model. This does not seem to have been observed in fractured rocks so far.

Fracture network models have been proposed and tested on field data (Robinson,1984; Long et al., 1985; Dershowitz, 1985) for flow calculations and in some cases also for tracer transport (Dverstorp, 1991; Cacas et al., 1990b). These models need information on fracture trace lengths, orientations, frequencies, transmissivities and the use of some assumptions which are difficult to prove. In the end they have to be calibrated to field observations.

We attempt a simpler approach in this paper and assume that flow and solute transport can be described as taking place in a network of channels. This simplification allows us to develop a simple model which does not need very detailed information. Data can be obtained from borehole transmissivity measurements and observations on fracture widths. Calibrations can be made with observations in drifts and tunnels. One of the important aspects of the present model is that it is simple enough to be able to accommodate the transport of sorbing solutes and especially solutes which diffuse into the rock matrix and sorb in the interior of the matrix. This is very important for the assessment of retardation of radionuclides which may escape from repositories for nuclear waste. Below we outline some observations which have been the basis for formulation of this model.

The flow in individual fractures is often assumed to be like flow between two parallel smooth plates. The relation between flow and pressure gradient will then be governed by the "cubic law". This has been experimentally shown for fresh fractures in granite (Witherspoon et al., 1980). Many natural fractures are old and weathered, filled with precipitated minerals or clays and cannot be expected to obey the cubic law. The pressure drop may more be determined by the physical size of the infilling material.

Analysis of tracer experiments between two boreholes in crystalline rock in three different experiments in Sweden indicate that the equivalent smooth plate fracture opening is very different from that obtained from the residence time data of the conservative tracers (Moreno et al., 1983, 1989).

Similar results were obtained by analyzing flow and solute movement in three different natural fractures intersecting tunnels in the granite in the Stripa mine (Abelin et al., 1985 and Abelin 1986). In this investigation it was also found that the same fracture when intersected by boreholes as close as 0.5 m distant had very different hydraulic properties. These observations indicated that the fractures were closed or very tight with less frequent open parts between the areas where the two fracture surfaces are in contact. Observations in drifts and tunnels strengthen this impression (Neretnieks, 1987a,b and Neretnieks et al., 1987).

The observed preferential pathways in a fracture plane may have several causes. In a fracture which has uneven surfaces, and where the aperture varies, the water will seek out the easiest paths for the prevailing gradient. The paths will change as the direction of the gradient changes (Tsang et al., 1988; Moreno et al., 1988). Such paths may be clogged or opened by chemical and erosion processes so that they are permanented in the fracture plane. Such chemical changes are frequently observed in old crystalline rocks where often several generations of fracture filling materials are found. Prominent dissolution channels have been found in fracture zones in Switzerland (Nagra, 1985). In two investigations (Neretnieks, 1987a; Abelin et al., 1987) it was found that fracture intersections often make up high flowrate conduits.

Fracture zones have so far not been investigated in the same detail as the regular rock mass. There are indications that some fracture zones may have very variable properties (KBS-3, 1983; Black et al., 1987). On the other hand in an experiment in a very prominent and very highly conductive fracture zone at Finnsjön in Sweden the hydraulic properties were within an order of magnitude in several bore holes (Ahlbom and Smellie, 1989).

An investigation in Stripa measured the hydraulic conductivity variations in fracture planes on the scale of 2 m. The results (Abelin et al., 1989) show that there are very strong variations in conductivity in the plane of the fractures.

The form of the channels and specifically the contact surface between the mobile water and the rock is of prime importance for the interaction of dissolved species with the rock. The interaction may be purely physical such as physical adsorption and diffusion into the rock matrix of solute molecules or it may be chemical such as ion exchange or precipitation.

In a field experiment performed in the Stripa mine by Abelin et al. (1987), water and tracer transport in granitic rock were studied. The test site consisted of a 75 m long main drift and a crossing arm 25 m in length and is shown in Figure 1. The ceiling and the upper part of the walls of the drift were covered by a total of 375 plastic sheets. Water flow into the drift in each plastic sheet was monitored for more than 2 years. These measurements showed that water flows into the drift with a very uneven spatial distribution.

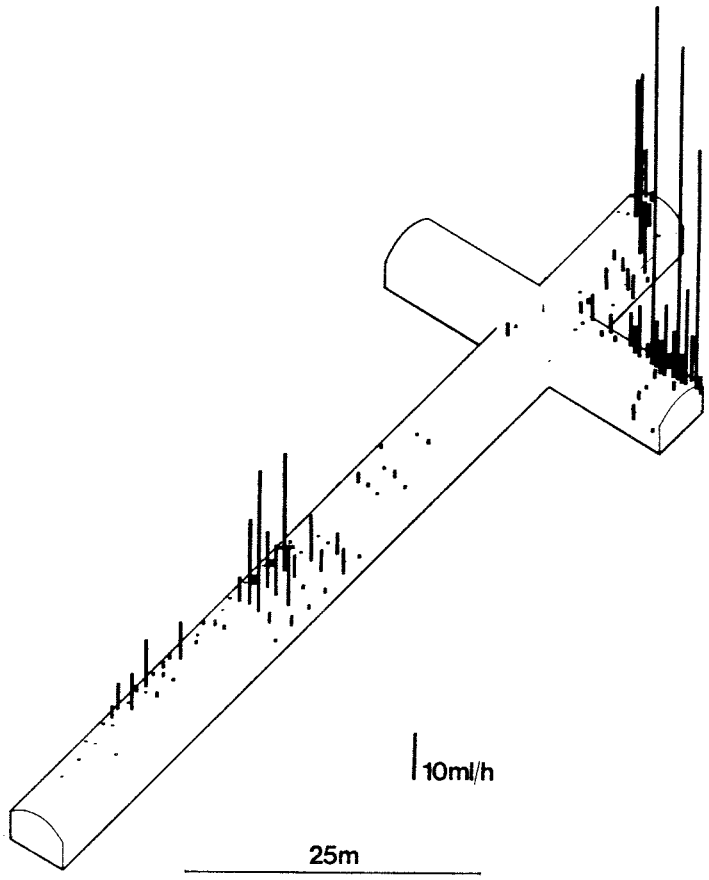


*Figure 1* A schematic view of the 3-D experiment in Stripa mine. Water flow rates into sampling sheets are also shown (Abelin et al., 1988).

11 different tracers were continuously injected in three boreholes at 9 different distances from the drift. The tracers flowing into the drift were recorded for about two years. The results show that the tracers are unevenly distributed in the drift. Very different concentrations were found in sheets near each other. Low values alternate with high values in nearby locations. In some cases, most of the tracer is found in locations far away from the injection hole.

Detailed observations of flow distributions in two other long drifts and tunnels, Kymmen (Palmqvist, 1987) and SFR (Neretnieks et al., 1987), show that the water outflow occurs in narrow channels, most of them less than 10 cm wide. The channel density (number of observed outflow spots on tunnel walls per area) is on the order of 1 per 20 to 100 $m^2$. Experiments specifically aiming to study channeling in individual natural fractures on the scale of 2-2.5 m in the Stripa mine (Abelin et al., 1988) also show that water is conducted in only a small part of a fracture. Channels have typical widths of less than 10 cm.

Porous media models can not describe this uneven flow distribution. Network models have been used to describe the flowrate distribution in the Stripa experiment (Herbert and Splawski, 1990; Geir et al., 1990; Dverstorp, 1991). They describe the stochastic nature of the areal flow distribution but do not account for the channeling nature of the flow. None of the models have addressed the question of interaction of solutes with the rock surfaces. Also none of the models have accounted for the observations (Abelin et al., 1989; Neretnieks, 1987) that fracture intersection play an important role in conducting the water solutes.

The fracture network models include the generation of fractures with a given geometry (e.g. circular fractures). The location of the center, diameter, aperture or hydraulic conductivity of the fractures are generated by stochastic methods. It is assumed that these entities are defined by some given distribution. The intersections between the fractures are determined and fluid transport in each fracture is calculated for given boundary conditions. In a recent study it was assumed that the flow in fractures which intersect each other may be described as the flow through channels in the planes of the fractures (Cacas et al., 1990a). These channels connect the centers of the fractures through a point at the intersection line between the fractures. In this case, the fracture network may be simplified to a network of channels which intersect each other.

One of the drawbacks of these models is that they need a very detailed data on fracture orientations, fracture size distributions and fracture conductivity distributions. It is assumed that all fractures or classes of fractures behave stochastically in the same way e.g. that all observed fractures are water conducting. Furthermore assumptions have to be made on the behaviour of the flow at fracture intersections and the solute mixing at the intersections. One additional difficulty is that it is necessary to use only a small fraction of the real number of fractures in the simulations because even the largest of present day computers cannot handle more information. The models with all their built in assumptions must finally be validated by comparison with field data.

## 2 CONCEPTUAL MODEL

In our approach a 3-Dimensional channel network model is developed which has the capability to account for the stochastic nature of the flow distribution, the channeling nature of the flow and the interaction of reactive solutes with the flow wetted rock surfaces.

To avoid many of the difficulties described above we take a different starting approach in our model. It is assumed that the flow paths make up a channel network in the rock. Every channel can connect to any number of other channels, but we take an upper limit of 6 channels intersecting in a point for reasons which are described later.

In each intersection up to six channels with different properties flow into or flow out from this point. Some of these channels or connections may have a very low conductivity which may represent no connection in the limit. The use of six channels is partly based on the observation that fracture intersection play an important role to conduct flow in addition to channels in the planes of the fractures. For two fractures which intersect there will be one channel in every fracture plane which may continue over the intersection line with the other fracture. In this way up to four members in the fracture plane may intersect in one node. For those intersections where the fracture intersection also is conducting two more members may be added forming a six member intersection. If there is more than one channel in a fracture an addition intersection point would exist.

Although the model concept is based on the above considerations it does not mean that we consider a channel to lie only in one fracture or at a fracture intersection. A channel in our concept may have formed by individual member channels in a series where the channels entering from the side to this linear element have a negligible flow compared to that in the "main" channel. A channel may thus consist of 1, 2, 3 or even more subchannels. The actual number is not very important as the properties of the channels will be obtained by calibration to field measurements. It would be good if many channels could be combined in this manner provided the important flow and transport properties could be maintained because the computation effort increases considerably with the total number of model channels used.

For visualization purposes the network is depicted as a rectangular grid with equally long channels. This does not reflect the real geometry of the channel network and can be distorted to account for the real geometry if one so wishes. The hydraulic properties of the members can be generated including the effects of different lengths of the channels, different hydraulic conductivities and other properties of interest.

It is easy to vary the channel density in different regions e.g. along fracture zones and to include effects of anisotropy in a simplified manner. In this paper we develop and test only some important basic properties of the model. They include the capability to describe the uneven spatial distribution of flow, the residence time distributions of tracers and the retardation due to matrix diffusion and sorption in the rock matrix.

Flow is simulated both for linear and convergent flow to account for the inflow to a tunnel such as in Stripa and to compare with the flowrate distribution there. Tracer transport is simulated in the same networks. For tracer transport additional information on channel volumes and flow wetted surfaces is needed. No independent data on this are available and therefore different assumptions are used and compared with the field results.

## 2.1 Flow in individual fractures

We do not think of the channels as necessarily being clearly identifiable physical features. In a fracture with varying apertures the water will trace out different paths depending on the gradient which exists at a given moment. When the conductivity variations are large there will only be one or a few paths where most of the water flows. This has been found in simulations (Moreno et al 1987,88 ) as well as in the field (Abelin et al 1989). The flowpaths may also be actual physical channels along fracture intersections or where dissolution processes have formed channels. They may have properties which vary along the flowpath, but an average conductivity, volume and flow wetted surface may be assigned to every channel. The individual channels form a network with at least three channels intersecting at a point. When only two channels meet the channel are thought to form one channel.

## 2.2 Stochastic nature of channels

All properties of the channels used in our model are thought to have a stochastic nature. The average transmissivity along the channel and the length of a channel define the conductance. This is the only entity needed to calculate the flow if the pressure difference between the two ends of the channel is known. The volume of the channels is needed in addition if the residence time is to be calculated for noninteracting solutes. For solutes which can sorb on the rock the "flow wetted" surface surface is needed in addition. If the rock matrix is porous and the solutes can have access to the interior porosity the matrix diffusion properties must be known in addition. We assume that it is possible to average these properties along a channel. Hydrodynamic dispersion in a channel as well as dispersion effects due to molecular diffusion in the mobile water are assumed to be negligible compared to the differences in residence times between channels. We assume that there is ideal mixing at fracture intersections.

## 2.3 Solute transport in single channels

The residence time distribution of the water and solutes, RTD, is determined by the volume of the channels in addition to the flowrate of the water. For solutes which can diffuse into the rock matrix or interact with the rock by sorption the "flow wetted surface" will play an important role also (Neretnieks 1980). Often the RTD is described in terms of a mean residence time and dispersion. The mean residence time is obtained from the first and the dispersion from the second moment of RTD. Higher moments

# 3 CALCULATION PROCEDURES

## 3.1 Generation of network

The fact that we use a rectangular network does not mean that the channels are of equal length or that they form such a network, but it is only a simple manner to visualize our network. Each member of the network is assigned a hydraulic conductance and for tracer transport also a volume and surface. The orientation and location of the members only becomes important when they are compared with a real geometry.

The flow calculations only need the information on the conductance of the channels and the boundary conditions. The conductance is defined as the ratio between the flow in a channel and the pressure difference between its ends. When solute transport is included the volume of the channel have to be known. If sorption onto the fracture surface or diffusion into the matrix will be included in the model, the surface of the channel (the flow wetted surface) must also be included. In the last case some properties of the rock are also needed such as rock matrix porosity, diffusivity, and sorption capacity for sorbing species.

In the present simulations the conductance of the channels is assumed to be lognormally distributed, with mean $\mu_0$ and standard deviation $\sigma_c$. The volume of the channel may be estimated in several ways. One is based on the assumption that the conductance in a channel is proportional to the aperture cubed. This is the often used notion of hydraulic aperture and would apply exactly for laminar flow in smooth parallel walled slits. Experimental observations have shown, however, that the aperture that determines the volume of the channels is not the aperture that determines the conductance of the channel (Witherspoon et al 1980, Abelin et al 1989). Different approaches will be discussed to estimate the volume of the channels. They will in addition be generated as being independent of the conductance and by using other non cubic relationships between conductance and volume.

For visualization purposes the volume of rock is divided in nodes in the three perpendicular directions. The center of each node is connected to the six neighbor nodes by channels with a given conductance. Figure 2 shows a schematic view of the mesh used in this report. The dimensions of the our system are denoted by Lx, and Ly in the horizontal plane and Lz in the vertical direction.

An outline of the approach used to calculate the fluid flow and solute transport through the network of channels is presented below. The method is described in more detail in (Moreno et al., 1988).

The rock volume is partitioned in cubic nodes. The centers of these nodes are connected by channels with different conductances. It is assumed that the conductances are lognormally distributed, and for the present study the grid is 20 x 20 x 20 nodes. It is also assumed that the conductance in the channels is not correlated in space.

which describe long exceptionally tails or early arrivals are usually not considered but especially the early arrivals may play an important role for decaying radionuclides.

There are several mechanisms which cause dispersion of tracers. Dispersion in the individual members of the network, dispersion caused by increase of the spread of residence times due to different velocities in the channels and spreading caused by matrix diffusion effects. In preliminary calculations we found that the dispersion in the individual members is negligible compared to the two other causes. This was also found by Cacas et al. (1990b). It will not be used further in this study.

Mixing at intersections will also influence the RTD of the network. There are several possible reasonable assumptions which can be made on the mixing processes (Robinson, 1984; Smith, 1987) but none of have been actually tested in real networks. In this study we assume that the fluids at an intersection mix fully.

Matrix diffusion effects and sorption in the interior of the matrix is assumed to be active and to be a Fickian process (Neretnieks, 1980).

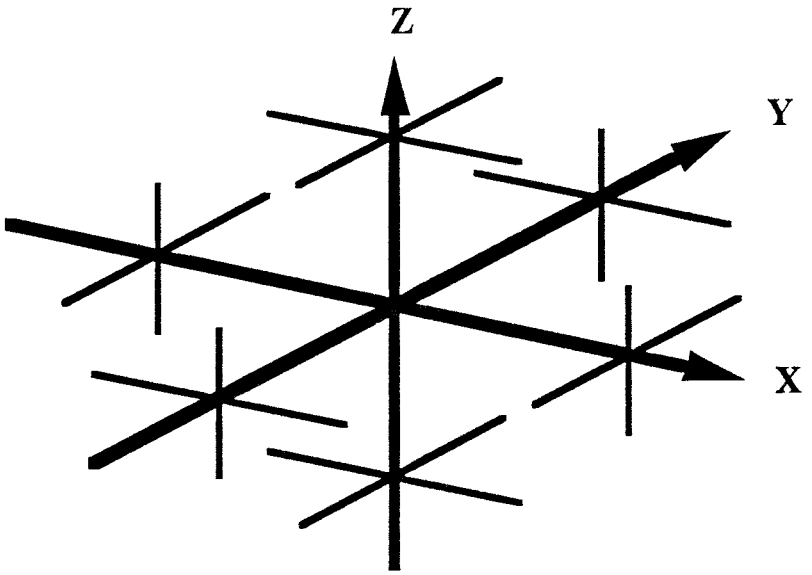


*Figure 2* A schematic view of the mesh used, each node is connected to up 6 other nodes.

## 3.2 Fluid flow calculations

For laminar conditions, the flow through a channel is proportional to the pressure gradient. In analogy with the Kirchoff law, the flow between two points "i" and "j" may be written as

$$Q_{ij} = C_{ij}(P_j - P_i) \tag{1}$$

where Cij is the conductance of the channel connecting the nodes "i" and "j". The pressure field is calculated by writing the mass balance at each intersection point:

$$\sum_j Q_{ij} = 0 \qquad \text{for all i} \tag{2}$$

The solution of this system of equations yields the pressure at each node. Flow between adjacent nodes is then calculated using Equation (1).

## 3.3 Solute transport calculations

The solute transport is simulated using a particle-tracking technique (Robinson, 1984; Moreno et al., 1988). Many particles are introduced, one at a time in the known flow field at one or more injection nodes. Particles coming to an intersection are distributed in the outlet channels with a probability proportional to the flowrates in the outlet channels. This is equivalent to an assumption of total mixing at channel intersections. Each individual particle is followed through the channel network.

The residence time in a given channel for nonsorbing tracers is determined by the total flow through the channel and its volume. The residence time of an individual particle over the whole path is determined as the sum of residence times in every channel that the particle has traversed. The residence time distribution is then obtained from the residence times of a multitude of individual particle runs.

From the RTD for individual particles, the mean residence time and variance can be calculated. The mean residence time and variance may be used to determine the Peclet number which is a dimensionless measure of the dispersivity. The dispersion may be expressed in terms of the variance in residence times, $\sigma_t^2$, of the breakthrough curve and is sometimes defined as a quantity that is inversely proportional to the Peclet Number, Pe (Levenspiel, 1972)

$$\frac{2}{Pe} = \frac{\sigma_t^2}{t_w^2} \tag{3}$$

The residence time for a particle in a channel is calculated from the volume of the channel and the flowrate. When dispersion in the channel and/or diffusion into the rock matrix are considered, different particles in the same channel will have different residence times.

Residence times for the particles in the channel may be described by the RTD of the particles expressed as a probability density function, pdf. It may be thought of as the outlet concentration for a pulse injection. If this curve is integrated over all the possible residence times the cumulative distribution of the residence times is obtained.

When diffusion from the moving water into and out of the rock matrix takes place a particle may reside in the matrix for some time in addition to its residence time in the water in the channel. For a flat channel from which the diffusion is linear and perpendicular to the channel surface a simple analytical solution is available for the RDT (Neretnieks, 1980). The outlet concentration for the solute in a channel or the cumulative curve, F, for the residence times is obtained from

$$F = \frac{c}{c_o} = \text{erfc}\left(\frac{(K_d D_e \rho_p)^{0.5} t_w}{(t - t_w)^{0.5} \delta}\right) \tag{4}$$

for times greater than the water plug flow residence time $t_w$, otherwise the concentration is zero. Equation (4) considers only advection in the channel and diffusion into the rock matrix. Longitudinal dispersion is neglected.

For a rectangular channel the water plug flow residence time may be calculated by $LW\delta/Q$. Introducing this expression into Equation (4) yields

$$F = \frac{c}{c_o} = \text{erfc}\left(\frac{(K_d D_e \rho_p)^{0.5} L W}{(t - t_w)^{0.5} Q}\right) \tag{5}$$

For particle tracking, we follow the technique used by Yamashita and Kimura (1990). The travel time for each particle in a channel is determined by choosing a uniform random number in the interval [0,1]. The travel time for the particle, t, is then calculated from Equation (6)

$$[R]_0^1 = \text{erfc}\left(\frac{(K_d D_e \rho_p)^{0.5} L W}{(t - t_w)^{0.5} Q}\right) \tag{6}$$

## 4 SOME PROPERTIES OF THE MODEL

More than 50 different flowrate simulations have been made for different standard deviations $\sigma_c$. Two different flow geometries have been used. In the parallel flow case flow is downward in a cube with nonflow boundaries on the vertical sides. Figure 3-a shows this case. Convergent flow is simulated approximately as shown in Figure 3-b.

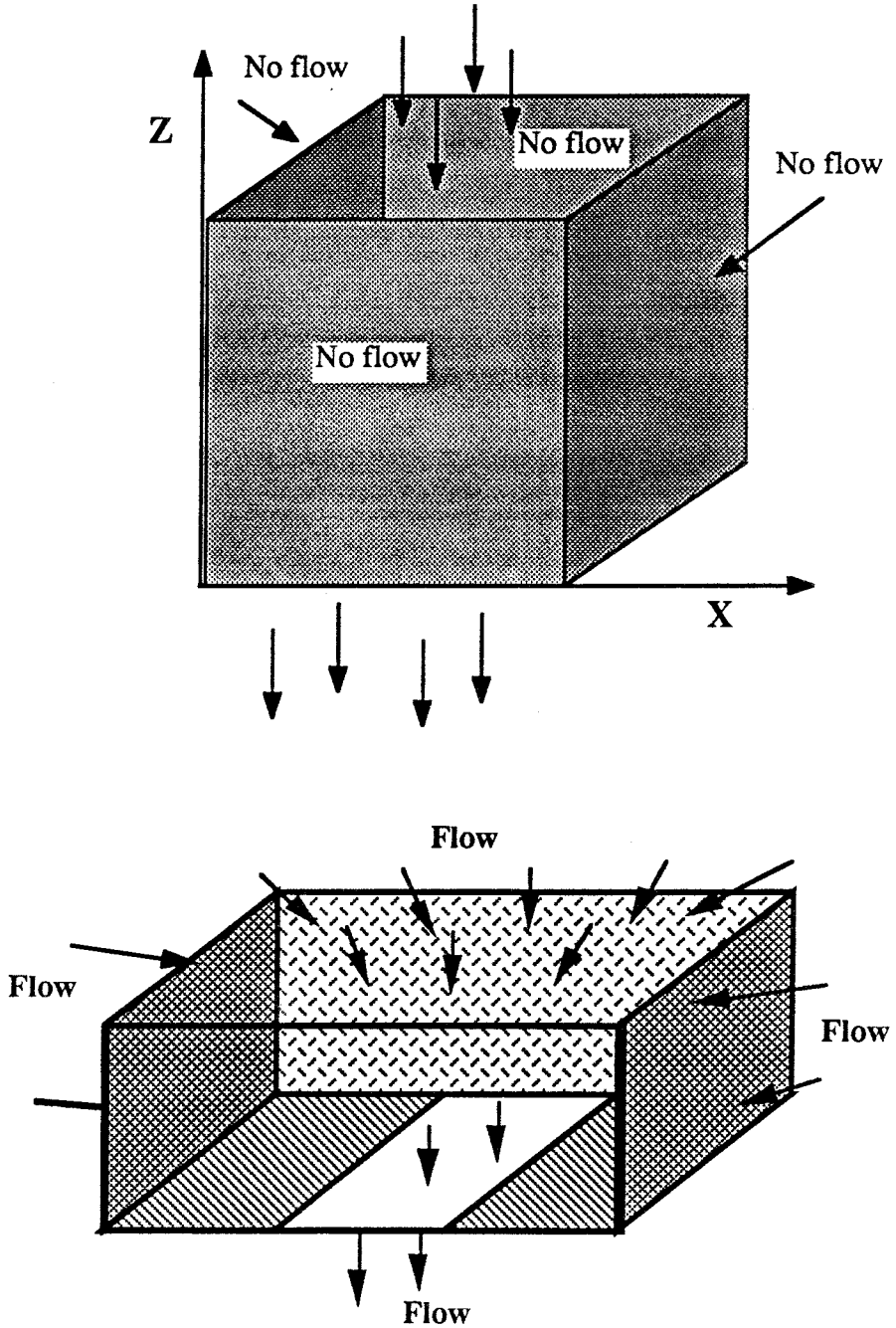


*Figure 3* Boundary conditions: a) for the parallel flow system, and b) for the "radially convergent" flow system.

## 4.1 Flowrate distributions

### 4.1.1 Linear flow

Figure 4 shows the number of channels of the 400 at the bottom of the grid, which carry a certain flowrate (relative ) for two different $\sigma_c$. Note that the flowrate decreases to the right in the diagram. The flowrates have been grouped in "bins" with the upper bound 2 times as large as the lower bound. This forms a geometric progression with a factor 2 between the bins. This mode of representation has been done because in practice the larger channels will always be seen whereas the measurement limit will determine how small flowrates will be observed. Figure 5 shows the fraction of flow in each "bin".

Figure 6 shows the cumulative number of channels and Figure 7 shows the cumulative fraction of flowrates as a function of the logarithm of decreasing flowrate. We note that the first 5-6 bins carry more than 90 % of the total flowrate.

The below type of diagrams will later be used to calibrate the model using field data.

Table 1 below shows the mean flowrate and standard deviation of flowrates $\sigma_q$ from the bottom of the grid for different standard deviations of the conductances $\sigma_c$. The flowrate distribution of the fluid flowing from the bottom was nearly lognormal. This was found by calculating the coefficients of skewness and kurtosis for the logarithm of the flowrates. The coefficient of kurtosis was small in most of the cases, less than 0.5 in absolute value. Only in a few cases, for large values for the standard deviation in the conductance distribution, the coefficient of kurtosis was about 0.8 - 0.9. The coefficient of skewness was between -0.7 and -0.2. A negative value of the coefficient of skewness signifies a distribution with an asymmetric tail extending out to smaller flowrates. For the simulations with a small $\sigma_c$, the flow distribution is closer to lognormal. Given the same logarithmic mean conductance the arithmetic mean flowrate and the total flowrate increases with increasing $\sigma_c$. The mean log flowrate decreases with increasing $\sigma_c$. This means that a few flow paths with high flowrate dominate the total flow in the channel network when the standard deviation of the conductance is large. The convergent flow results are very similar to those for parallel flow.

It may be noted that the standard deviation of flowrates $\sigma_q$ from the bottom of the grid is 10 - 15 % lower than the standard deviations of the conductances $\sigma_c$.

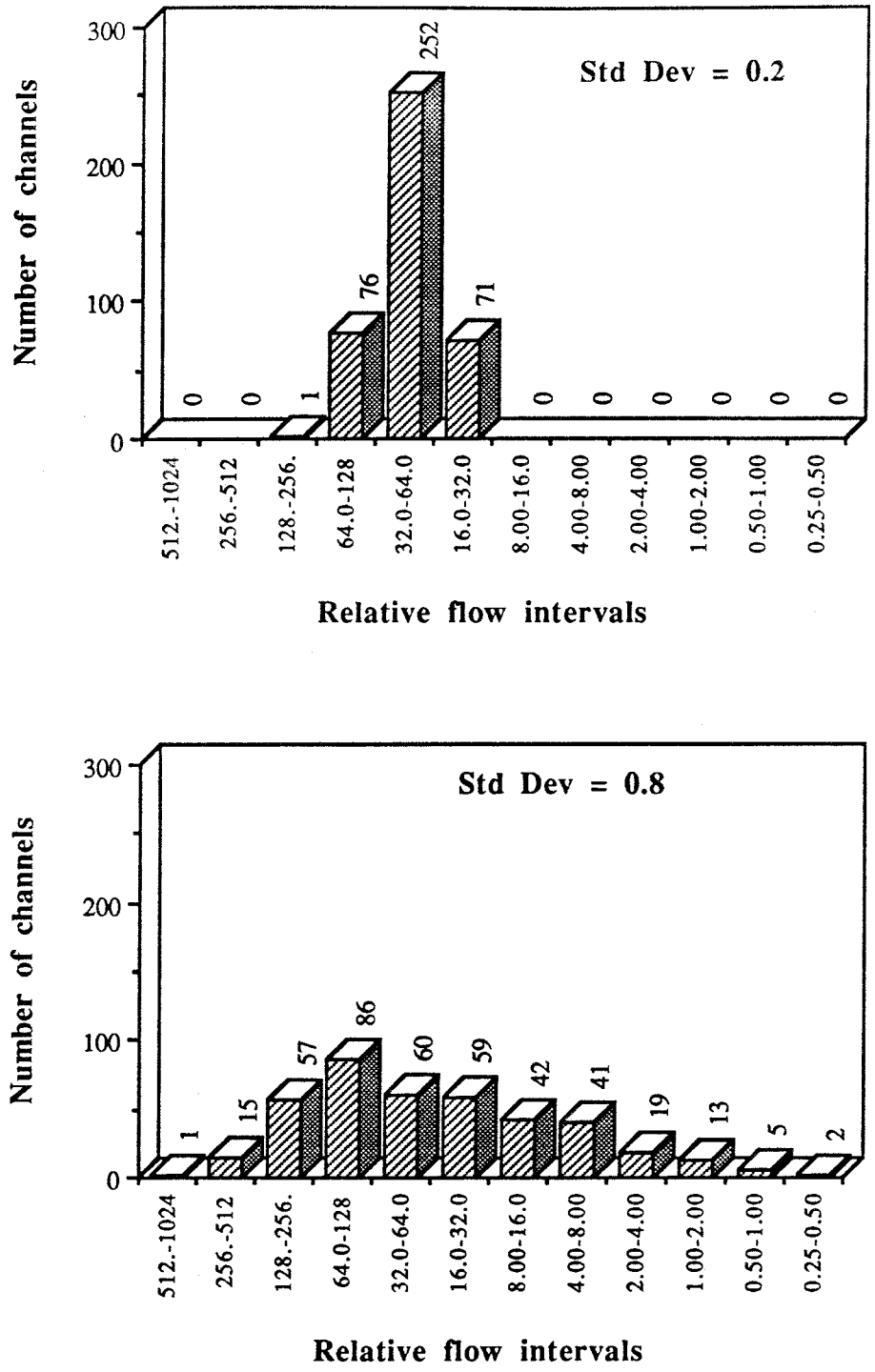


*Figure 4* Histograms for the number of channels with flowrate in a given interval. For a value of 0.2 (a) and 0.8 (b) in the standard deviation of the conductance $\sigma_c$.

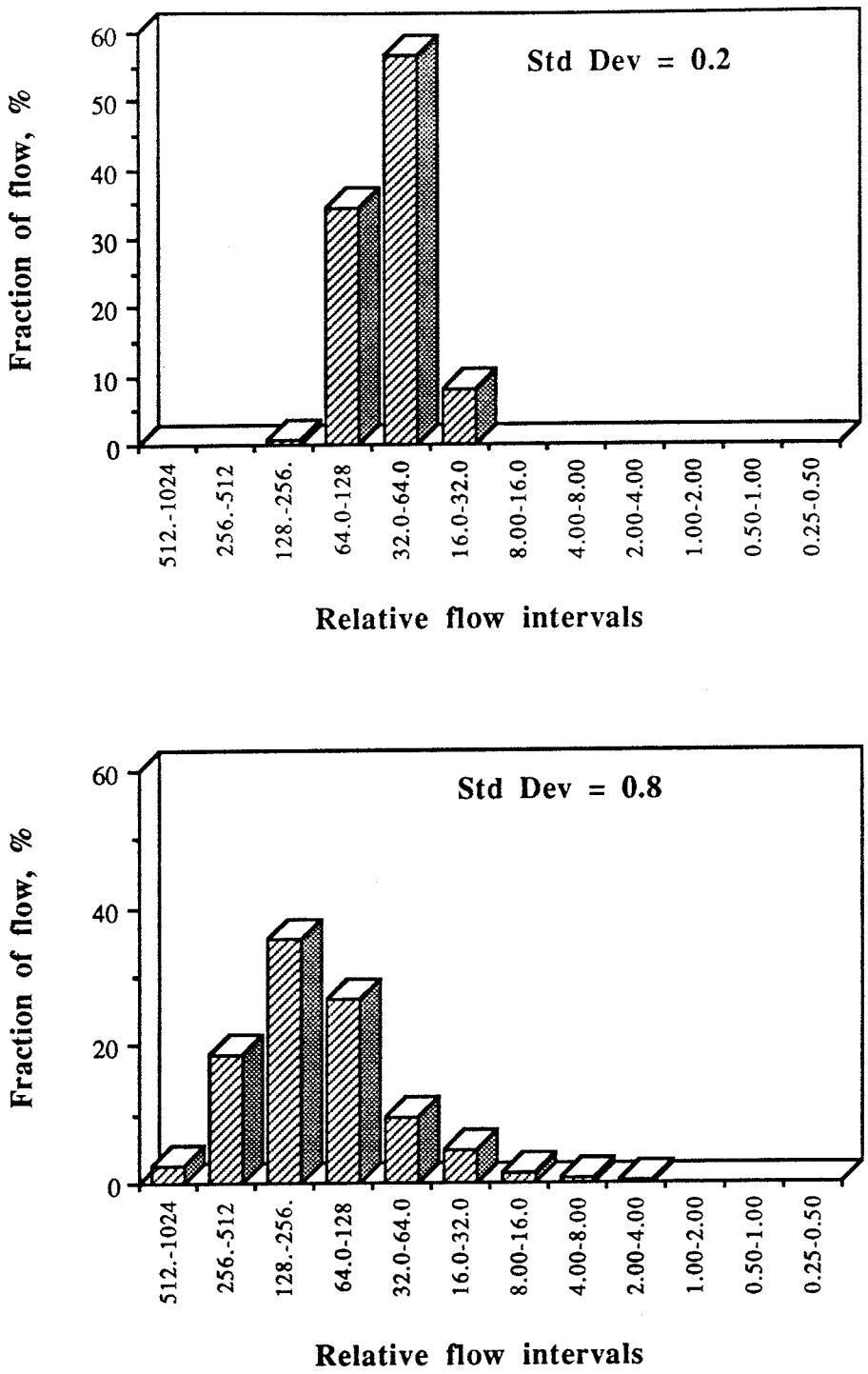


*Figure 5* Histograms for the fraction of the total flowrate for channels with flowrate in a given interval. For a value of 0.2 (a) and 0.8 (b) in the standard deviation of the conductance $\sigma_C$.

a)

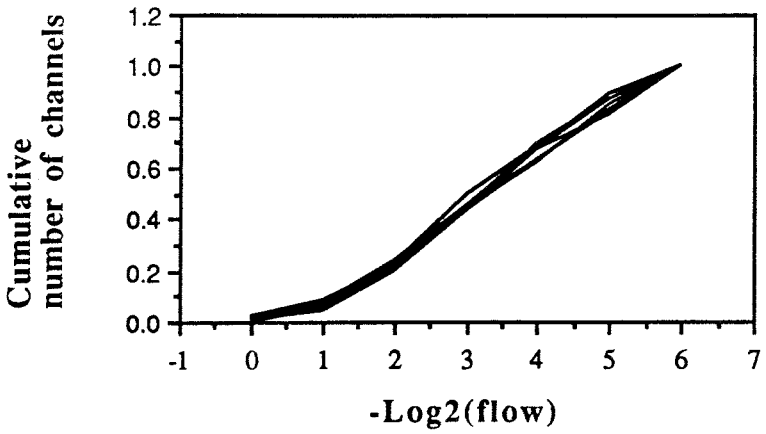


b)

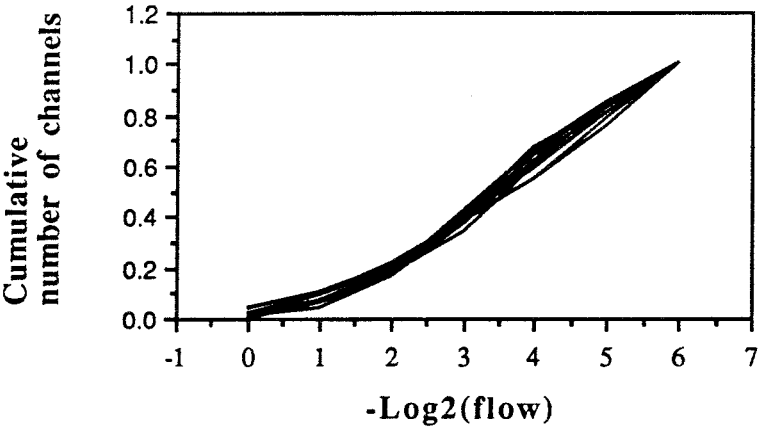


c)

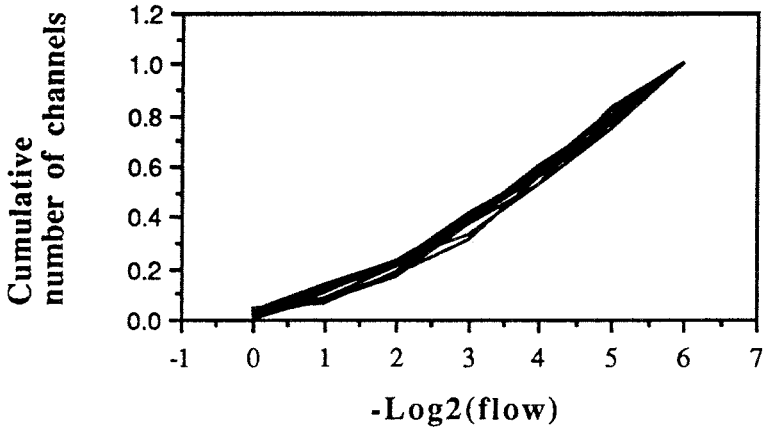


*Figure 6* Cumulative number of channels as a function of decreasing flowrate for different $\sigma_c$ a) 0.8, b) 1.6, and c) 2.4.

a)

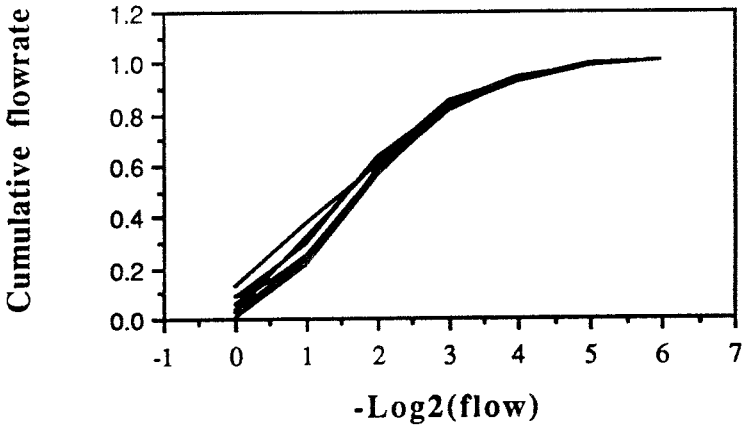


b)

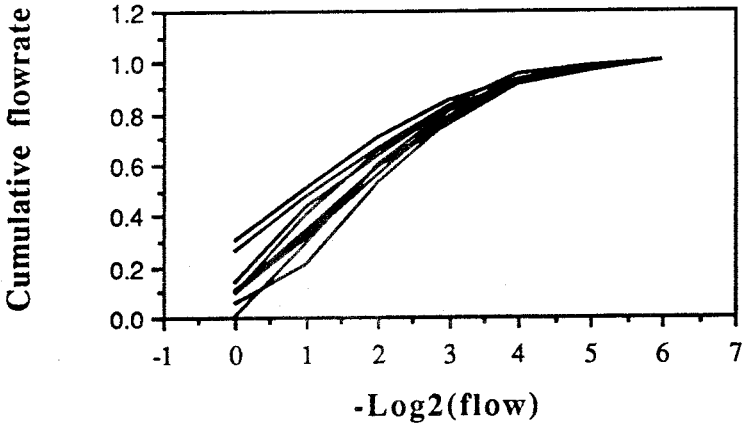


c)

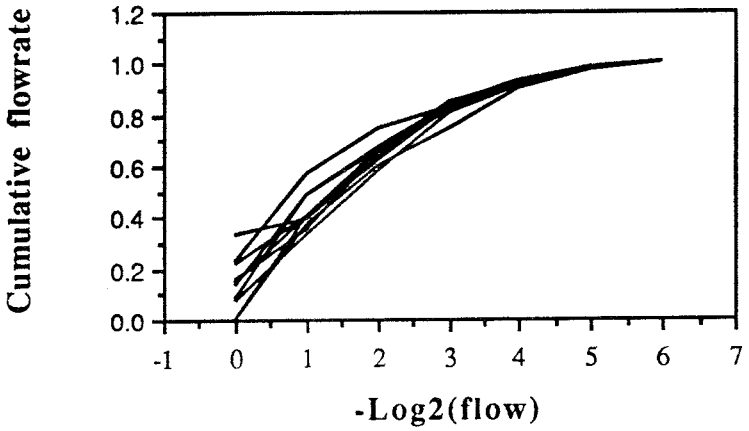


*Figure 7* Cumulative fraction of flowrates as a function of decreasing flowrate for different $\sigma_c$ a) 0.8, b) 1.6, and c) 2.4.

*Table 1* Flowrate from the bottom. Arithmetic mean flowrate and mean, standard deviation, and skewness for logarithm of flowrate.

| Standard deviation $\sigma_c$ | Mean flowrate (rel unit) | Mean log-flowrate | Standard. deviation $\sigma_q$ | Coeff. of skewness |
|---|---|---|---|---|
| Parallel Flow | | | | |
| 0.0 | 1.00 | 1.00 | 0.00 | - |
| 0.1 | 1.01 | 1.00 | 0.08 | (*) |
| 0.2 | 1.04 | 0.97 | 0.16 | -0.25 |
| 0.4 | 1.14 | 0.88 | 0.33 | -0.43 |
| 0.8 | 1.51 | 0.65 | 0.66 | -0.60 |
| 1.2 | 2.18 | 0.43 | 1.00 | -0.67 |
| 1.6 | 3.34 | 0.27 | 1.34 | -0.69 |
| 2.4 | 8.51 | 0.10 | 2.01 | -0.70 |
| 3.2 | 33.20 | 0.04 | 2.71 | -0.70 |
| Convergent Flow | | | | |
| 0.0 | 1.00 | 0.97 | 0.11 | 0.78 |
| 0.1 | 1.01 | 0.96 | 0.13 | 0.32 |
| 0.2 | 1.03 | 0.93 | 0.19 | -(*) |
| 0.8 | 1.53 | 0.63 | 0.67 | -0.55 |
| 1.6 | 3.45 | 0.27 | 1.35 | -0.66 |
| 2.4 | 7.77 | 0.09 | 2.04 | -0.69 |

(*) skewness shows positive and negative values.

Figure 8 shows the standard deviation of flowrates in the vertical channels $\sigma_q$ at some intermediate distances between inlet and outlet for $\sigma_c$ =1.2. It is seen that $\sigma_q$ in the interior locations is lower by some 20-30 % than at inlet and outlet. This is caused by the fact that a constant head is imposed at the boundaries whereas the heads at the interior points adjust themselves to the local resistances.

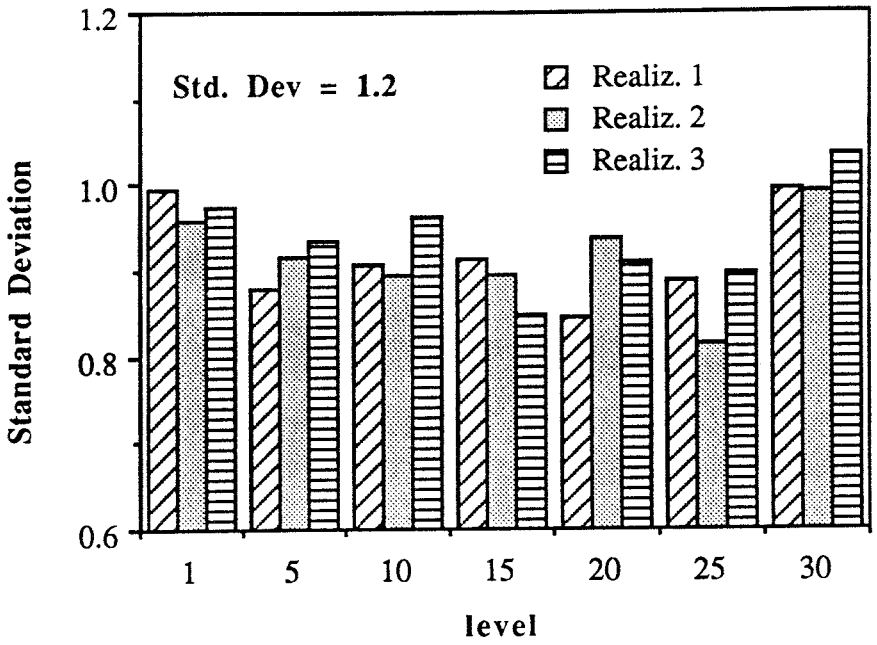


*Figure 8* Standard deviation of the flowrates in the direction of the regional gradient as a function of the location level. Level 1 corresponds to the bottom and level 30 to the mesh at the top. Water flow is downward. Results for 3 realizations. Standard deviation of conductances $\sigma_c$=1.2.

### 4.1.2 Convergent flow

The convergent flow was simulated by changing the mesh and the boundary conditions. The new mesh is 40x20x15 nodes (horizontal length, width, height). The new boundary conditions are: constant head on the top of the rock volume and in the vertical sides at x=0 and x= Lx. No flow conditions at the vertical sides at y=0 and y=Ly. On the bottom no flow condition was assumed, except on a rectangle along the y-axis 10 nodes in width, where constant head was assumed. This means that 200 flow channels are found on the bottom. The boundary conditions for this case are shown in Figure 3-b.

We have defined constant head on the top and on two vertical surfaces, the real boundary conditions would be constant head at a long distance from the center of the tunnel. Moreover, our system is not radially symmetric. The boundary conditions and geometry used play an important role for simulations with small standard deviation, where the flow distribution is strongly influenced by them. For example, for a mesh with equal conductances ($\sigma_c$ = 0.0) the flow distribution has a standard deviation of 0.11 instead of a value of 0.0 (value that would correspond to a radial symmetric geometry). For large $\sigma_c$, the effect of the boundary conditions becomes negligible. This is seen in Table 1, where for large values of $\sigma_c$ the standard deviation in the flow

distribution, $\sigma_q$, also is about 0.8 times $\sigma_c$, showing the same relationship as that for parallel flow. For small $\sigma_c$ the value of $\sigma_q$ is in some cases greater than $\sigma_c$.

For convergent flow, the spatial distribution of the flowrates into the drift is similar to the distribution obtained when a regional parallel flow is modelled, if $\sigma_c$ is large. For small values of $\sigma_c$ the spatial flow distribution is determined by the boundary conditions as discussed above.

## 4.2 Number of "active" channels at intersections

The number of channels which carry a significant fraction of the total flow will decrease with increasing standard deviation of conductances $\sigma_c$. To explore the number of channels at each intersection which contribute significantly to the total flow the following procedure was used.

The curve for conductance distribution (lognormal) was divided into 6 intervals along the axis of log conductances, where each part has the same area under the curve (1/6). Then, on the average, the channel with the smallest conductance in an intersection will belong to the first of these intervals, and the channel with the largest conductance will belong to the last interval. We consider as negligible a conductance which is 1 % of the lowest limit of the largest conductance interval defined above (83.3 % in the cumulative curve) and we calculate the fraction of intersections that has a given number of channels with non-negligible conductance. For example, for a standard deviation of 1.6, 39 % of the channels have a conductance which is less than our limit. From this value we determine that 5, 20, and 32 % of the intersections have 6, 5 and 4 channels respectively. It may also be determined that 75 % of the intersections have 4 or less active channels. These values were checked with simulated results for a grid of 20x20x20 nodes and the agreement was excellent. Results for different standard deviations are shown in Table 2. The connectivity of the channel network is strongly reduced when the standard deviation of the conductances is increased. A large standard deviation of conductances will result in a network with sparse channels in the above sense.

*Table 2* Fraction of intersections with a given number of channels, for different standard deviations in the conductance distribution.

| Number of Channels | Standard Deviation 0.40 | 0.80 | 1.60 | 2.4 |
|---|---|---|---|---|
| 0 | 0,000 | 0,000 | 0,004 | 0,029 |
| 1 | 0,000 | 0,000 | 0,033 | 0,139 |
| 2 | 0,000 | 0,000 | 0,130 | 0,281 |
| 3 | 0,000 | 0,004 | 0,268 | 0,301 |
| 4 | 0,000 | 0,046 | 0,316 | 0,183 |
| 5 | 0,000 | 0,273 | 0,199 | 0,059 |
| 6 | 1,000 | 0,676 | 0,052 | 0,008 |

## 4.3 Sensitivity to the parameters used

The distribution used in the generation of channel conductances is defined by two parameters: the mean and the standard deviation of log conductance. The influence of the standard deviation in the conductance distribution was discussed above. The mean of the log conductance is only a scaling factor which would be adjusted to match the mean flowrate in an experiment or field observation.

For regional parallel flow, we mostly used a mesh with 20 x 20 x 20 nodes. If a mesh of very large size is used, without any correlation between the conductance of the channels, the solute transport through the channel network is expected to become equivalent to transport through a homogeneous porous medium. On the other hand, for a very small mesh the influence of the different conductances in the channels will be very strong, i.e. the channeling effect is increased. This would be the case for transport through short distances or through rock masses with few fluid pathways. This point will be discussed later together with solute transport.

At present only the effects of the mesh size on the flow distribution are discussed. Simulations were made using different mesh sizes. The number of nodes in the direction of the pressure gradient used were 10, 20 and 40 nodes keeping 20 times 20 nodes in the other directions. No significant differences were found in the flow distribution in these cases. Also, a mesh with 10x10x10 was used and quite similar results were found.

## 4.4 Solute residence time distributions for noninteracting solutes

At a given time, many particles are injected in a point in the mesh and the particles reaching the outlet are collected at their respective locations. The mass flow at a given location is proportional to the number of particles which reach that location per time unit. The relative concentration is determined from the number of particles per time unit that arrive at a collection point divided by the flowrate in the same location.

For each location with a large enough number of particles (larger than 25) the Peclet number and mean residence time are calculated. To obtain plots of breakthrough curves for a pulse injection the particle tracking is done using many particles and quite large time intervals. Fewer particles are needed to simulate a step injection. This is carried out by summation of all the particles which have an arrival time less than a given time. This is the approach used in the present study.

For solute transport calculations the channel volume is needed to determine the travel time for the tracer (or particles) through the channel network. There are no reliable relationships known at present between the transmissivity of channels and their volume. Several approaches are explored. The volume of the channels could be determined from a new *independent distribution* (e.g. a new lognormal distribution). This means that the volume of the channels would be totally independent of its conductance. Another choice is to use the *hydraulic aperture*, calculated from the values of conductance assuming laminar flow in parallel walled channels to calculate the volume of the channels. There is, however, experimental evidence that this is not the case for tight channels. The small apertures (constrictions) play an important role in the determination of the conductance while the large apertures determine the channel volume.

The main difficulty to determine which of the possible approaches may represent the real channel volume is the lack of data. We have tested some approaches between conductance and volume for a channel. From these simulations, we expect to find which approach(es) could be used by comparisons with field observations of tracer residence time distributions.

Four different approaches were chosen:

- Volume calculated from the *hydraulic aperture* using the cubic law.

- Aperture assumed to be *proportional* to the hydraulic conductivity, e.g. channels with filling material.

- Volume determined from an *independent* random distribution.

- Volume assumed to be *constant*.

For channels with equal length and width the volume is proportional to the aperture raised to power 3 in the hydraulic aperture assumption. In the proportional approach it is assumed that the conductivity is proportional to the aperture, this would be the case if the channel is filled with filling material which causes the pressure drop.

In the independent conductance approach, the volume is randomly generated assuming the channel volumes are lognormally distributed. The standard deviation in the channel volume distribution is taken to be equal to: a) $\sigma = \sigma_c/3$ and b) $\sigma = \sigma_c$. In the constant approach, we assumed a constant channel volume.

The interval in which the channel volume may be found as a function of channel conductances is compared for the different approaches. For example, for a given standard deviation in conductance ($\sigma_c = 1.2$). 95 % of the channel conductances are found within a span of 5 orders of magnitude. Then for the cubic law approach the channel volumes are found in a quite narrow interval (about 1.5 orders of magnitude). For the proportional approach, this interval spans 5 orders of magnitude. Figure 9 shows the relationship between conductance and volume and the possible intervals where channel volumes may be found for a standard deviation of 1.2.

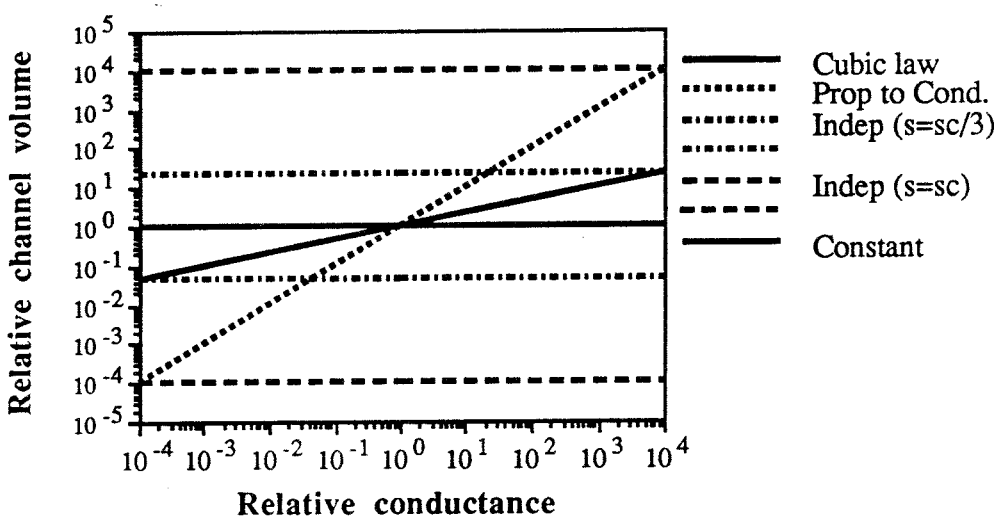


*Figure 9* Channel volume as a function of the channel conductance for the different approaches used in the simulations of solute transport.

Solute transport simulations were made as follows. For a mesh 20 x 20 x 20, with downward flow, the injection was made at level 15 from the bottom. Travel times for particles flowing into each collection section were recorded, and breakthrough curves were obtained by summing the number of particles which have a travel time less than a certain time. This curve corresponds to the outlet concentration as a function of time for a step injection. From the travel time distribution, the Peclet number at each collection section is determined.

The largest dispersion was found for the independent volume approach with a large standard deviation for the volume distribution. Peclet numbers were less than 5 in all the simulations. The smallest dispersion was found for the cubic law approach. Some outflows show a quite large dispersion, Pe<1. When it was assumed that all the channels have the same volume the dispersion was quite large. Peclet numbers for the different cases are shown in Figure 10 for a standard deviation in channel conductances of 1.2.

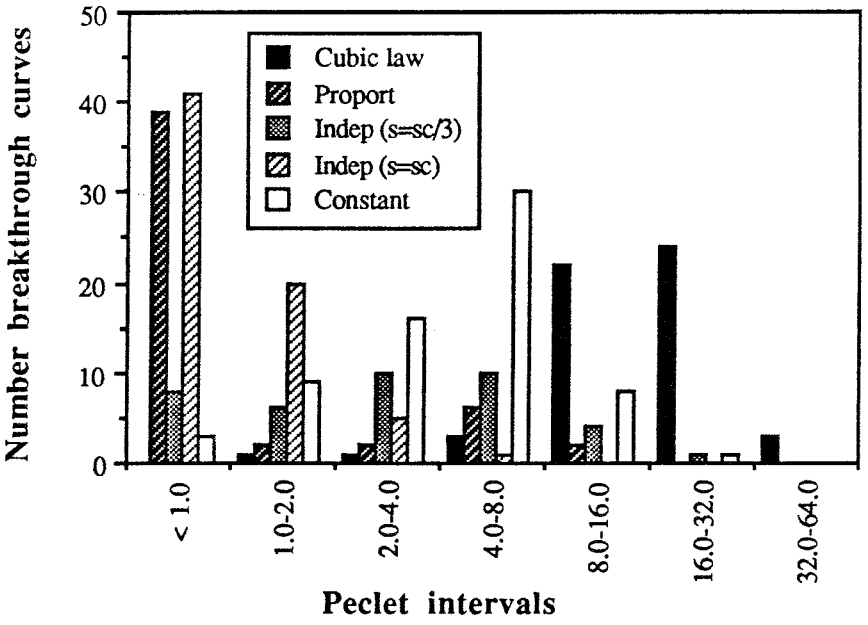


*Figure 10* Histogram showing the Peclet number for the different approaches using a standard deviation in channel conductances of 1.2.

Breakthrough curves formed by collecting all the particles (from all 400 channels) flowing from the bottom into one stream were also determined for the different approaches. Peclet numbers, calculated from these curves, show the same trend as discussed above. The cubic law approach gives the smallest dispersion. The largest dispersion is found when the channel volumes are independent of the conductance. Generally the breakthrough curves show a long tail and in some cases plateaus are also found indicating distinct multiple channels. Some breakthrough curves obtained using the cubic law are shown in Figure 11.

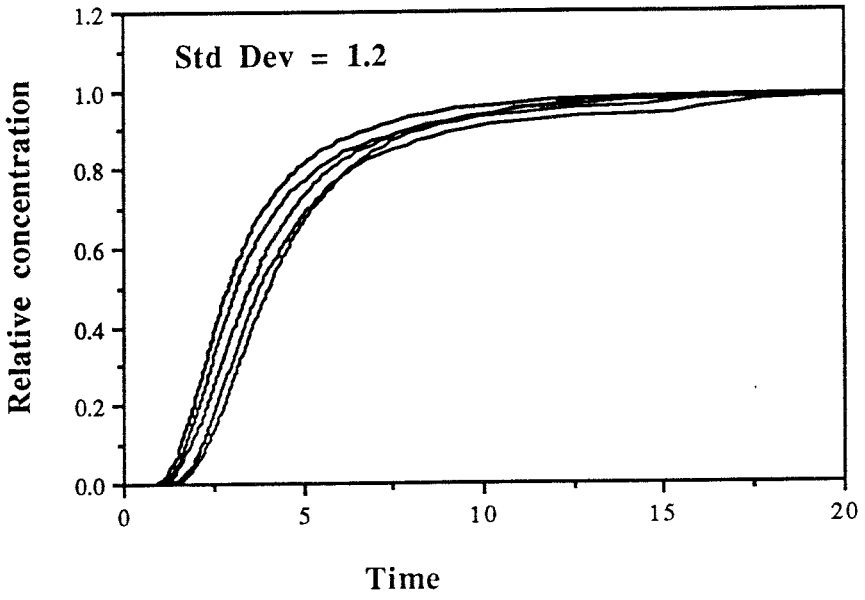


*Figure 11* Some typical breakthrough curves formed by collecting all the particles from all channels at the outlet for a standard deviation of 1.2 in conductance and using the hydraulic aperture approach.

Figure 12 shows Peclet numbers and residence times as a function of the distance between injection and the different collection points for the approach where the volume of a channel is proportional to the hydraulic conductivity (cubic law). No clear correlation is found between Peclet number and travel distance either between residence time and travel distance taken as the shortest distance between injection and collection points.

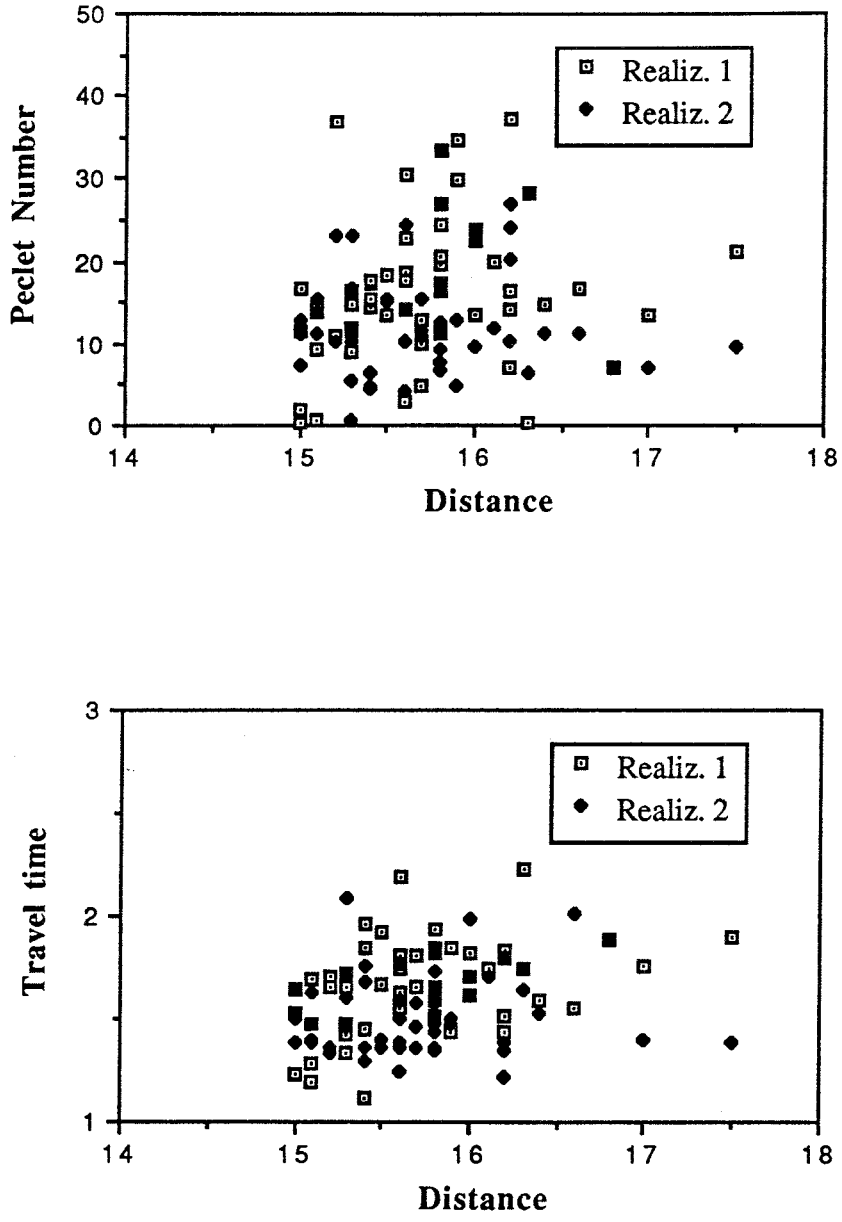


*Figure 12* Peclet number and residence time as a function of the travel distance for the approach where the volume of a channel is proportional to the hydraulic conductivity. Results from two realizations. Standard deviation in conductance of 1.2.

The collection sections where the injected tracers (particles) reach the drift are illustrated by plotting its spatial distribution. Figure 13 shows the maximum concentration at different locations for small ($\sigma_c$ = 0.2) and large ($\sigma_c$ = 1.2) standard deviation in conductance. The maximum mass flow is shown in Figure 14. The maximum mass flow is proportional to the number of particles which come to one location.

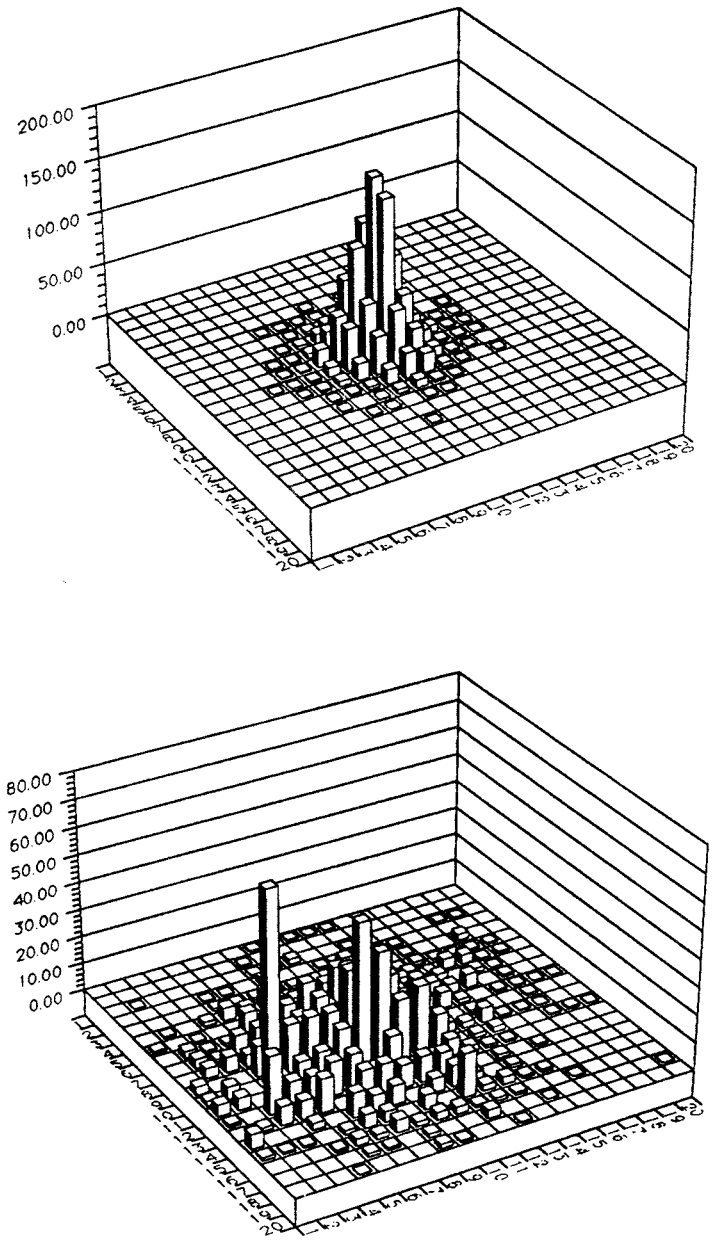


*Figure 13* Spatial distribution of the maximum concentration for a value of 0.2 (a) and 1.2 (b) for the standard deviation of the conductance $\sigma_c$.

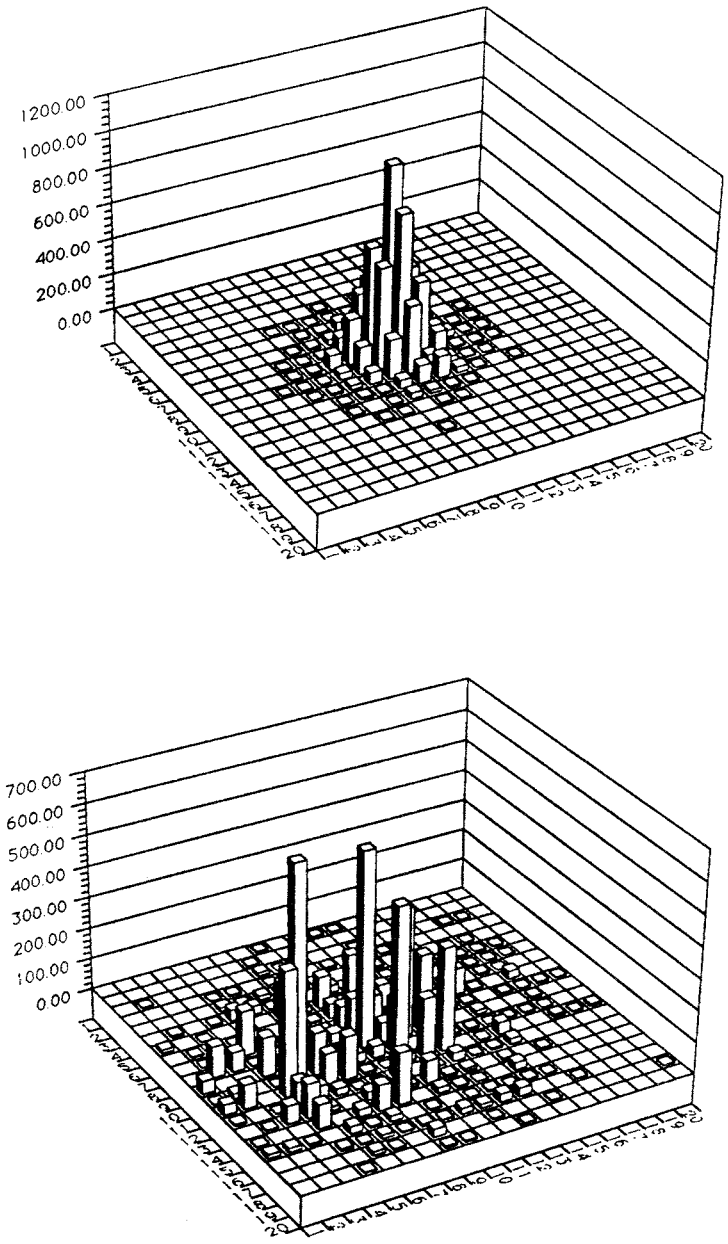


*Figure 14* Spatial distribution of the maximum mass flow rate for a value of 0.2 (a) and 1.2 (b) for the standard deviation of the conductance $\sigma_C$.

When a small standard deviation is used the spatial distribution of concentration is narrow, with a maximum value under the projected injection point. The concentration decreases rapidly with the distance from the projected injection point. For a large standard deviation, the maximum concentration shows some isolated peaks. These results show that flow in channels with different conductivities may explain the variations of concentration with the location. Low concentrations may be found surrounded by high concentrations or vice versa.

The spatial distribution of the mass flow shows that for a low standard deviation most of the mass (particles) comes to points under the injection. For a large standard deviation, many peaks are found. The mass flow is to some extent determined by the distribution of the fluid flow so it is not surprising that its distribution is very uneven for large standard deviations.

The influence of the standard deviation of the channel conductance on dispersion was also explored. The dispersion is calculated from the breakthrough curve collecting all the particles. Generally, the curves are smooth and have long tail, only a few curves show a partial plateau. Figure 15 shows the Peclet numbers as a function of the standard deviation of conductance. The curves show the median and upper and lower 10 percentiles, obtained from 54 simulations. The Peclet number has a maximum for $\sigma_c$ around 0.8.

Figure 15 also shows the residence time for the same set of curves. The residence time increases with the standard deviation in conductances if they are normalized to the same total flowrate.

The sensitivity of the results for solute transport to the grid size was also explored. Grid sizes of 20, 30 and 40 were used for comparison. For large values of $\sigma_c$ the differences are not significant when the grid is increased from 20 to 40 channels in the direction of the flow. Possibly a much larger grid is needed to get a smoothing in concentration or/and increase the Peclet number. Figure 16 shows Peclet number as a function of the travel distance in the flow direction from the injection point located at the 5th level from above. The lines show the limits for the upper and lower 10 percentiles. The Peclet numbers are typically in the range between 5 and 30 in these simulations where the cubic law assumption was used to obtain the channel volumes

No significant increase of the Peclet number with the length of the grid is observed. Similar results are found for total breakthrough curves. For networks generated with a low $\sigma_c$ the dispersion decreases somewhat when the length of the network is increased in length.

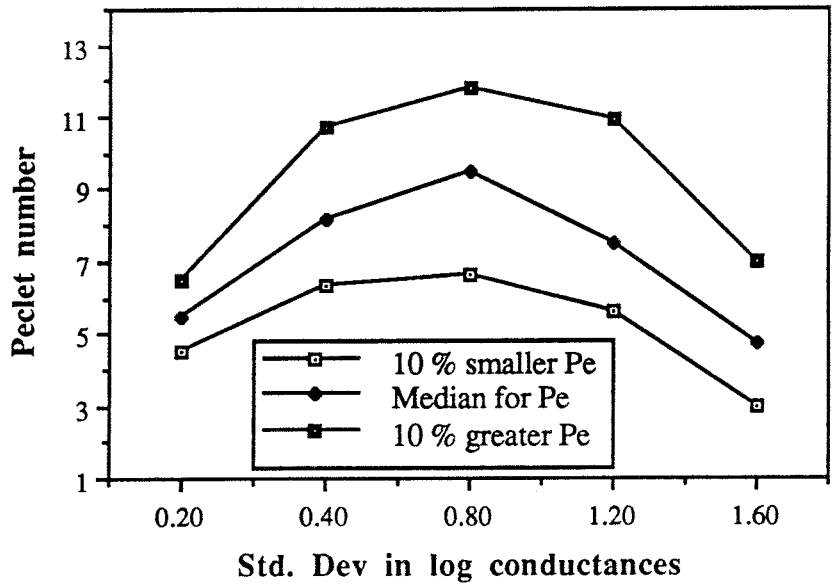


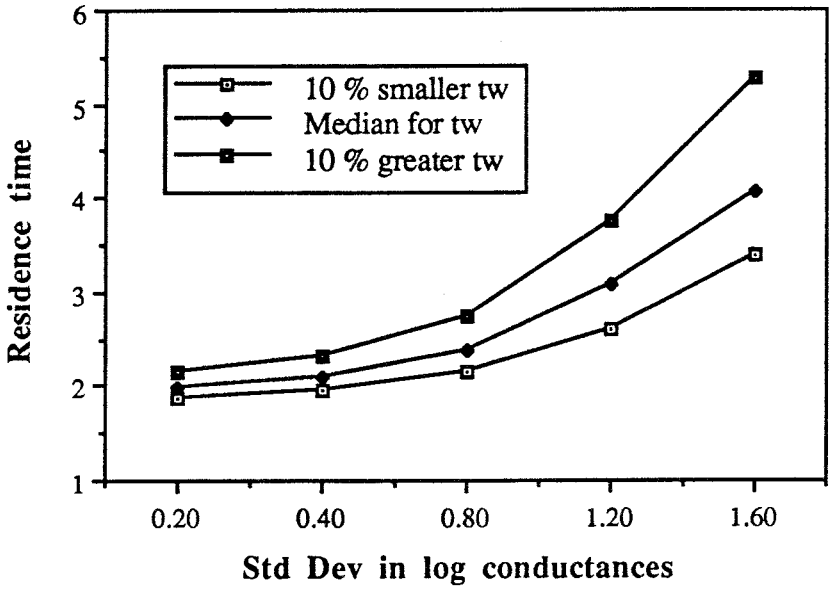


*Figure 15* Peclet number and residence time for different standard deviations in conductance for the approach with channel volume determined using the cubic law.

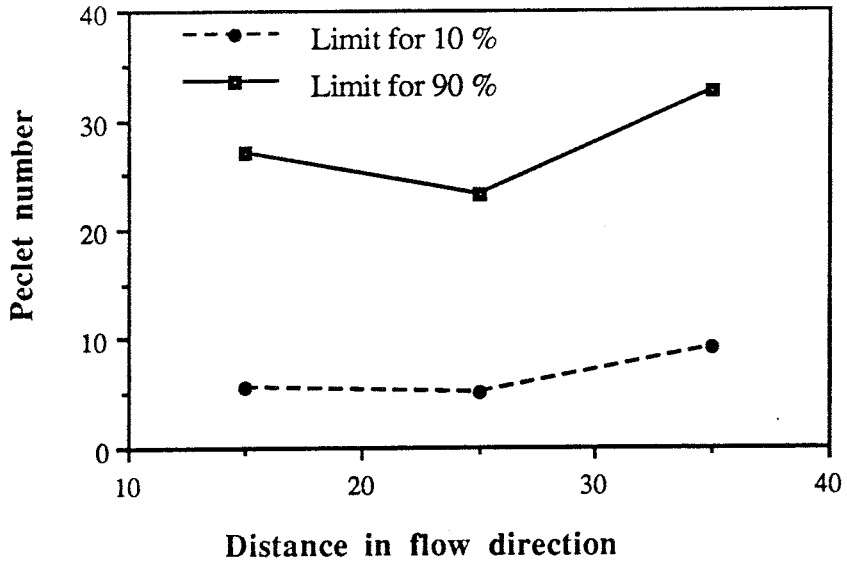


*Figure 16* Peclet number as a function of the travel distance for different lengths of the grid in the direction of the flow. Standard deviation in conductance of 1.2.

## 4.5 Matrix diffusion

If diffusion into the matrix is also accounted for the residence times of the particles in the channels are larger than the residence time without diffusion into the matrix. The residence time for each particle that passes the channel is stochastically determined by Equations (5) and (6).

The capability of the particle tracking method to describe the diffusion in the rock matrix was tested generating a channel network with equal channels (zero standard deviation). The channel thus consists of 15 subchannels in series with equal properties. In this channel, we used the stochastic process to simulate the diffusion in the rock matrix.

The results are compared with the analytical solution. The results agree well if some thousand particles are used. For few particles (hundreds), differences of about 5 % are obtained. Figure 17 shows the breakthrough curves for a path formed for 15 channels in series with the same volume and conductivity and the analytical solution for the same case. The procedure was found to be fast and accurate also in network calculations.

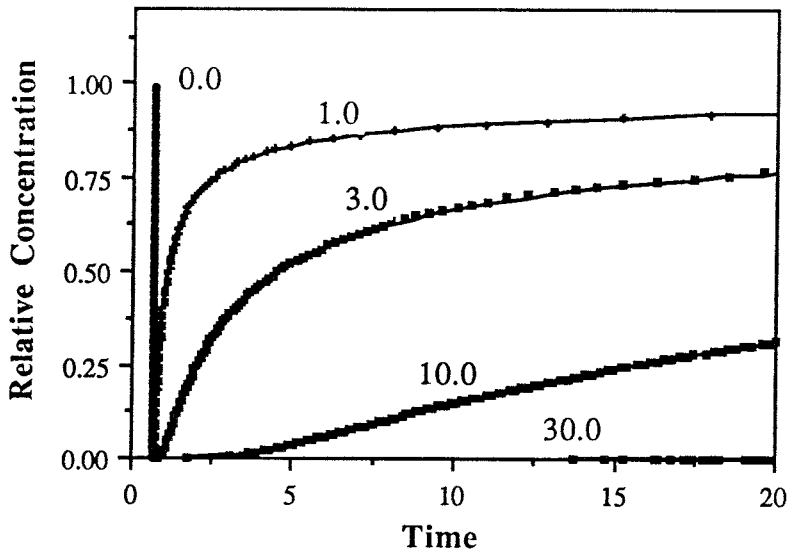


*Figure 17* Breakthrough curves when there is diffusion in and sorption within the rock matrix. Comparison of analytical solution and particle tracking results. 8 000 particles were used. The number on the curves is proportional to the flow wetted surface.

# 5 CALIBRATION AND COMPARISON WITH FIELD OBSERVATIONS

The calibration is done in the following way. For the inflow measurements to the drifts cumulative inflow data are compared with the simulated results such as in Figure 7. This gives an estimate of the standard deviation of conductances $\sigma_c$. Thereafter the cumulative number of observed channels are compared to those obtained by simulation as in Figures 6. As will be discussed below the field results often have observations over only 1.5-2 orders of magnitude in flowrates. The cumulative number of channels which have been found in the field up to the smallest flowrate are then proportioned to obtain the "total" number of channels in the model sense. Equation (7) below shows the procedure.

$$\frac{\text{Total \# channels in rock}}{\text{Total \# channels used in simulation}} = \frac{\text{Cumul \# channels observed in rock}}{\text{Cumul \# channels in simulations}} \qquad (7)$$

The same procedure can be used for the packer test data if these are analysed for the number of intersections provided channel widths and the borehole diameter are known. This will be described later.

The channeling network model gives no inherent information on channel widths or lengths. Also the distribution function for the conductances of the channels is not known a priori. For the latter we assume that it is log normal and it then suffices to determine the mean and standard deviation by fitting to measured data. It has been found by several investigators that the standard deviation of transmissivities obtained in boreholes is often between 1 and 3 on the base 10 log scale (Cacas, 1990a; Holmes et al., 1990; Geier et al., 1990). Dverstorp (1991) used $\sigma_c$ values ranging from 0.4-2.4 in simulations of the Stripa experiments with best results for $\sigma_c$=1.7. Cacas et al., (1990a,b) found a value of $\sigma_c$=3.2 for the Fannay Augere experiments in their fracture network model calibration.

## 5.1 Using data from drifts and tunnels

At the SFR Site there are flowrate measurements available of individual spots over an area of 14 000 $m^2$ (Neretnieks, 1987). Table 3 below summarizes the data.

The flowrate ranges have been chosen on a geometrical progression such that each range "bin" is half as large as the previous and they have been ordered in decreasing progression. The reason for this is that undoubtedly one will observe the largest flowrate spots but will have a decreasing accuracy in detecting spots with lower flowrates. It generally is also not possible to know the total inflow to the low flowrate spots so that a cumulative flowrate curve cannot be constructed starting at the low flow end. However, a cumulative curve can be started from the high flowrate end and can be compared to the model results. If diagrams like those in Figure 7 are used and the

experimental results plotted in those, an estimate of the standard deviation of conductances can be made. It may be noted that the cumulative flowrate increases little when more than 5-6 "bins" are used. The method can thus be expected to be robust in the sense that the most important paths have been accounted for. For the SFR data $\sigma_C$ is found to be about 1.6 using this method.

*Table 3* Flowrate distribution in the different spots at SFR

| Flowrate range l/min | Number of spots | Cumulative number of spots |
|---|---|---|
| >=1.6 | 2 | 2 |
| 0.8-1.6 | 4 | 6 |
| 0.4-0.8 | 12 | 18 |
| 0.2-0.4 | 41 | 59 |
| 0.1-0.2 | 38 | 97 |
| >0.1 | 67 | 164 |

Having established $\sigma_C$ the number of channels can be found by "aligning" the two columns, "Model number of channels" and "Observed number of channels" starting with the highest flowrate range matching as in table 4 below. In the table three different $\sigma_C$ columns are given.

From the table it can be seen that the model and observed results agree best for $\sigma_C$=1.6. This is also seen in Figure 18 where the 3 rightmost columns have been plotted in a histogram. It is seen from the figure that the bars for $\sigma_C$=1.6 have more even heights than the other, meaning that the observed and model distribution agree best for this $\sigma_C$.

The average ratio of the model to observed spots was fond to be 1.36 meaning that the model has 36 % more spots than the real drifts and cavern at SFR. As the model has 400 channels the SFR has 400/1.36=294. Every spot thus has 47.6 $m^2$ on the average and the length of the channels on average is the square root of this figure, Z=6.9 m.

*Table 4* Match of model and observed flowrates at SFR.

| | Cumulative number of channels from model for | | | Observed channels | Ratio Model/Observed number of channels | | |
|---|---|---|---|---|---|---|---|
| $\sigma_c$= | 0.8 | 1.6 | 2.4 | | 0.8 | 1.6 | 2.4 |
| Flowrate category | | | | | | | |
| 1 | 4 | 2.7 | 1.9 | 2 | 2.00 | **1.35** | 0.95 |
| 1/2 | 16 | 11 | 10 | 6 | 2.67 | **1.83** | 1.67 |
| 1/4 | 72 | 33 | 21.5 | 18 | 4.00 | **1.83** | 1.19 |
| 1/8 | 148 | 68 | 40 | 59 | 2.51 | **1.15** | 0.68 |
| 1/16 | 220 | 107 | 61 | 97 | 2.27 | **1.10** | 0.63 |
| 1/32 | 278 | 145 | 87 | 164 | 1.70 | **0.88** | 0.53 |
| 0 | 400 | 400 | 400 | | | | |
| Average | | | | | 2.52 | **1.36** | 0.94 |
| Max/Min | | | | | 2.4 | **2.1** | 3.1 |

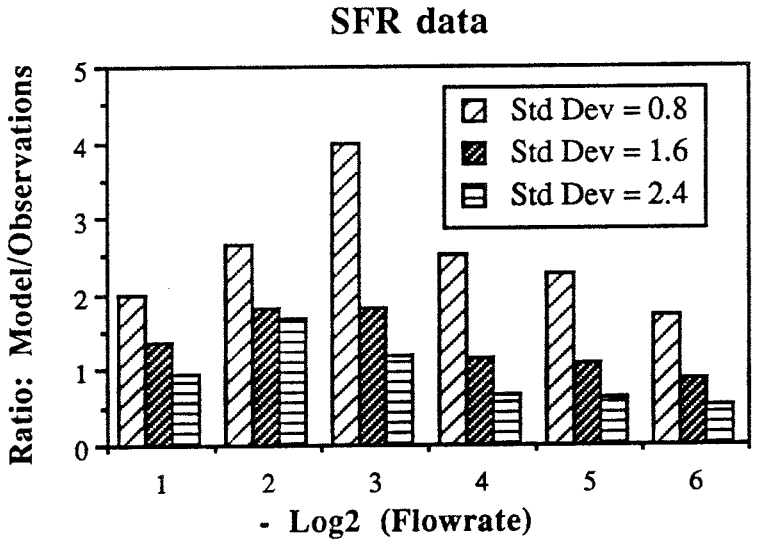


*Figure 18* Ratio of model to observed number of channels in SFR for different $\sigma_c$.

The same method can be applied to the observations in Stripa assuming that every sheet has only one channel. Table 5 below summarizes the results.

*Table 5* Match of model and observed flowrates at Stripa.

| | Cumulative number of channels from model for | | | Observed channels | Ratio Model/Observed number of channels | | |
|---|---|---|---|---|---|---|---|
| $\sigma_c$= | 0.8 | 1.6 | 2.4 | | 0.8 | 1.6 | 2.4 |
| Flowrate category | | | | | | | |
| 1 | 4 | 2.7 | 1.9 | 1 | 4.00 | 2.70 | **1.90** |
| 1/2 | 16 | 11 | 10 | 7 | 2.29 | 1.57 | **1.43** |
| 1/4 | 72 | 33 | 21.5 | 14 | 5.14 | 2.36 | **1.54** |
| 1/8 | 148 | 68 | 40 | 26 | 5.69 | 2.62 | **1.54** |
| 1/16 | 220 | 107 | 61 | 40 | 5.50 | 2.68 | **1.53** |
| 1/32 | 278 | 145 | 87 | 59 | 4.71 | 2.46 | **1.47** |
| 1/64 | 320 | 179 | 111 | 79 | 4.05 | 2.27 | **1.41** |
| Average | | | | | 4.48 | 2.38 | **1.54** |
| Max/Min | | | | | 2.49 | 1.72 | **1.33** |

Figure 19 shows the ratio columns for Stripa in the same way as was done for SFR.

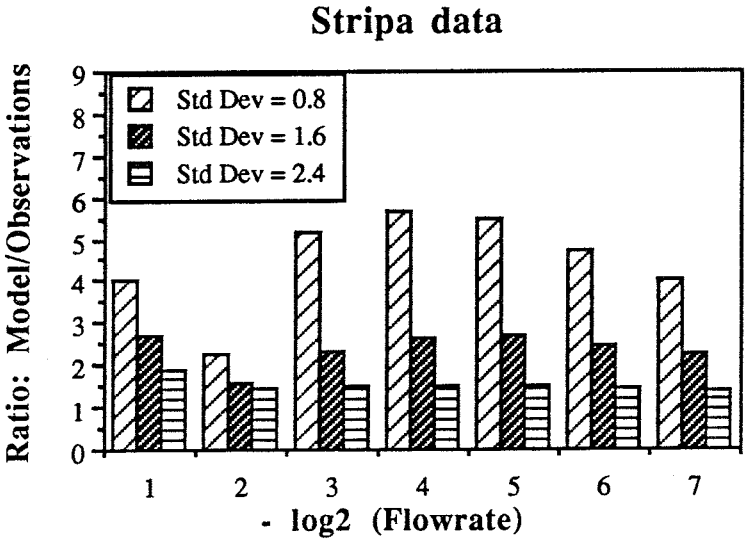


*Figure 19* Ratio of model to observed number of channels in Stripa for different $\sigma_c$.

The best agreement is obtained for $\sigma_c$=2.4 found both by matching with Figure 7 and in Table 5. For Stripa the number of channels are 400/1.54=260 and they have an average are of 2.9 $m^2$ and a length of 1.7 m.

In addition to the quite detailed Stripa and SFR measurements there are flowrate estimates in spots in a drilled tunnel at Kymmen in west Sweden (Neretnieks, 1987). The Kymmen tunnels is a 4.5 km long full face drilled tunnel with a diameter of 4.6 m. It traverses gneiss-granite, gneiss-granite with amphibolite, leptite and amphibolite. 63 fracture zones were identified making up a total length of 672 m or 15 % of the length of the tunnel. In the fracture zones 181 individual flowing spots were charted and in the rock mass outside the zones 206 spots were found. The flowrate range above slowly dripping spots was from 0.01 to 6.5 l/min. The flowrates were grouped in 4 categories by the drift mappers: V2 (0.01-0.2), V3 (0.2-1.5), V4 (1.5-6.5) and V5 (>6.5 l/min).

A comparison is made with the model results which have been grouped in the same relative flowrate categories. This is shown in Table 6.

*Table 6* Match of Model and observed flowrates at Kymmen.

| | Cumulative number of channels from model for | | | Observed channels | Ratio Model/Observed number of channels | | |
|---|---|---|---|---|---|---|---|
| $\sigma_c$= | 0.8 | 1.6 | 2.4 | | 0.8 | 1.6 | 2.4 |
| Flowrate category | **Rock mass exclusive zones** | | | | | | |
| V4 | 16 | 11 | 10 | 2 | 8.00 | 5.50 | 5.00 |
| V3 | 220 | 107 | 61 | 81 | *2.72* | *1.32* | ***0.75*** |
| V2 | 380 | 213 | 160 | 206 | *1.84* | *1.03* | ***0.78*** |
| | | | | Average | *2.28* | *1.18* | ***0.76*** |
| | **Zones** | | | | | | |
| V5 | 4 | 2.7 | 1.9 | 4 | 1.00 | 0.68 | 0.48 |
| V4 | 72 | 33 | 21.5 | 8 | *9.00* | *4.13* | ***2.69*** |
| V3 | 278 | 145 | 87 | 63 | *4.41* | *2.30* | ***1.38*** |
| V2 | 393 | 260 | 180 | 181 | *2.17* | *1.44* | ***0.99*** |
| | | | | Average | 5.19 | 2.62 | **1.69** |

In Table 6 the largest category has been omitted in the averaging as indicated by the italicized figures. The bold figures indicate best agreement. The number of channels in the rock mass is 400/0.76 =526 with an average area of 100 $m^2$ and a length Z=10.2 m. For the zones the number of channels are 237, the area per channels is 41 $m^2$ and Z=6.4 m. It may be noted that on the average the zones have 2-3 channels over their width.

Table 7 summarizes the results for the three sites.

*Table 7* Summary of the results for SFR, Stripa and Kymmen

| | $\sigma_c$ | A $m^2$ | Z(drift) m |
|---|---|---|---|
| SFR | 1.6 | 47.6 | 6.9 |
| Stripa | 2.4 | 2.9 | 1.7 |
| Kymmen rock mass | 2.4 | 100 | 10.2 |
| Kymmen zones | 2.4 | 41 | 6.4 |

Channel widths have been observed in drifts and tunnels. Recently Palmqvist and Lindström (1991) analysed the earlier observations in the Kymmen tunnel and found that 99.7 % of the channels have a width smaller than 0.1 m. Channel widths at SFR also were mostly a few tens of cm at most with a few exceptions. Also a large number of them were point spots found at fracture intersections and as small holes (Neretnieks 1987). At Stripa in the 3D drift it was also found that the water collection sheets collected more water in areas where there were more fracture intersections (Abelin et al., 1987). A recent experimental investigation specifically measuring channeling at Stripa (Abelin et al., 1989) also found that channels typically were a few centimeters to a few tens of centimeters wide. We use 10 cm as a "typical "width for channels in this paper.

## 5.2 Using borehole data to estimate channel lengths

The number of conducting channels would be equal to the number of fracture intersections if all fractures were more conductive than the rock matrix. As even the rock matrix is made up of small crystals with microfractures between and them the number of conducting fractures is very large. In practice the measurement limit in packer tests will determine when a packer section is assumed to be "nonconducting". Typically the transmissivity of the most conducting sections in the rock mass are 4-6 orders of magnitude more transmissive than the measurement limit. The measurements are typically available in the form of a number of packer intervals with measured

transmissivities for the borehole tests and flowrates from a number of channels into drifts. These can be used to estimate the total number of conductive fractures (channels) intersected by the borehole(s). This has been done on data from Stripa (Geier et al., 1990). There then remains to translate this information into the number of channels of a certain width W and length Z per rock volume. A method to do this is developed below.

### 5.2.1 Channel length

The rock contains a large number of channels which have an average length Z and an average width W as shown in Figure 20.

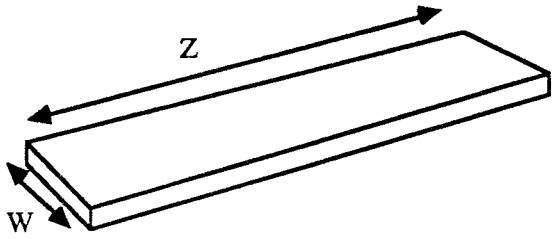


*Figure 20* Definition of length Z and width W of a channel.

If there are a number of such channels in a volume of rock a borehole which is drilled in the rock may intersect some of them. In this analysis we assume that the aperture of the channels is very small compared to the other dimensions of the channel and also that the widths of the channels are small in relation to the average distance between channels.

Consider a borehole with diameter $D_{bh}$ and how a channel must be located in order to be in contact with the hole. Figure 21 shows the vertical borehole and a channel with different angles to the horizontal.

The average distance is obtained by integrating over all angles $\alpha$. It is

$$W_{av} = \frac{1}{\pi/2}\int_0^{\pi/2} W \,\mathrm{Sin}\,\alpha \, d\alpha = W\frac{2}{\pi} \qquad (8)$$

In the same way the average distance in the other direction $Z_{av}$ can be obtained at which a channel will intersect the hole. This is illustrated in Figure 22.

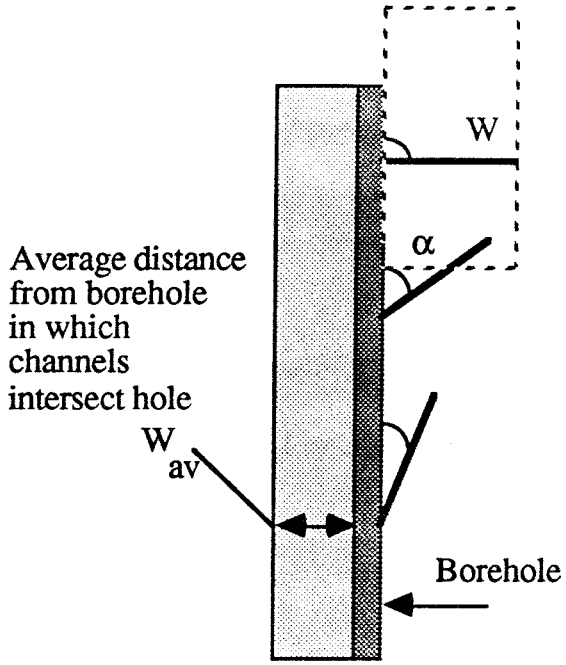


*Figure 21:*
Showing the average distance at which the "outside" of the channel can be and still touch the borehole.

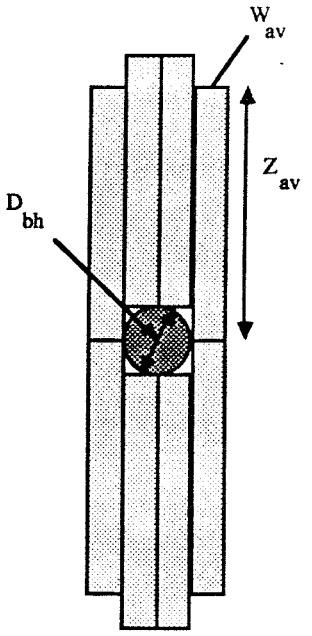


*Figure 22:*
View of borehole from above indicating at which distance from the borehole a channel must lie on average in order to be in contact with a borehole.

The average length of the channel is obtained analogous to the width Equation (8) and Figure 21 and becomes

$$Z_{av} = \frac{1}{\pi/2}\int_0^{\pi/2} Z \,\mathrm{Sin}\,\beta \, d\beta = Z\frac{2}{\pi} \qquad (9)$$

Thus the area in Figure 22 in which a channel must lie on the average to contact the hole is

$$A_{av} = \frac{\pi}{4} D_{bh}^2 + 2\, Z_{av} (D_{bh} + 2\, W_{av}) \qquad (10)$$

If the average distance between channels intersected by the borehole has been obtained to be L then the rock volume containing one channel is $L*A_{av}$. In a system with a cubic grid of channels every cube with sides Z is delimited by 12 channels. Every channel is shared by four other cubes so there are three channels per a volume of size $Z^3$. Thus

$$Z^3 = 3\, L\, A_{av} = 3\, L \left(\frac{\pi}{4} D_{bh}^2 + 2\, Z_{av} (D_{bh} + 2\, W_{av})\right) \qquad (11)$$

Inserting Equations (8) and (9) into (11) gives

$$Z^3 = 3\,L\,A_{av} = 3\,L\left(\frac{\pi}{4}D_{bh}^2 + 4\frac{Z}{\pi}\left(D_{bh} + 4\frac{W}{\pi}\right)\right) \qquad (12)$$

If L, $D_{bh}$ and W are known from independent measurements then Z is obtained from equation (12). When $Z>>D_{bh}$ the first term in equation (12) can be neglected and Z is obtained from

$$Z^2 = L\,\frac{12}{\pi}\left(D_{bh} + 4\frac{W}{\pi}\right) \qquad (13)$$

### 5.2.2 Results from borehole observations

Geir et al., (1990) found that in 3 horizontal North-South oriented boreholes drilled nearly parallel to the 3D drift in Stripa the standard deviation of transmissivities was 1.5 (10Log) and the conductive fracture frequency was 0.57 $m^{-1}$. In two horizontal East-West oriented boreholes starting at the 3D drift the same values were found for the fracture density and the standard deviation. The mean transmissivity, however, was 10 times higher in the latter holes.

Using a width W=0.1 m and a borehole diameter of 0.076 m Equation (13) above gives an average channel length of Z=1.2 m. This agrees reasonably well with the results obtained from the observations of flowrate distribution in the 3D drift Z=1.7 m.

## 5.3 Residence time distributions from tracer tests

The approaches used to describe the relation between channel volumes and conductances cover a wide range of assumptions ranging from an approach where the volume is directly related to the conductance, to an approach without any correlation between volume and conductance. In the Stripa tracer tests the majority of the breakthrough curves gave Peclet numbers less than 4 although for one of the tracers in Stripa large Peclet numbers, on the order of 20 were found. The low Peclet numbers would not favor the cubic law relation. or the constant volume assumption. However, no clear conclusion may be obtained from these simulations with the existing experimental data. This is a point which must be studied in more detail both theoretically and experimentally.

The Stripa tracer experiments also gave information on the porosity which was in the range $0.2\text{-}1.5\cdot10^{-4}$ for the different tracers. The average was $0.6\cdot10^{-4}$. The porosity of our model rock is

$$\varepsilon_f = \frac{3\,W\,b}{Z^2} \qquad (14)$$

With channels 0.1 m wide and 0.1 mm in aperture the porosity of our rectangular grid is $0.2 \cdot 10^{-4}$ for Z=1.2 m and $0.1 \cdot 10^{-4}$ for Z=1.7 m. Considering that the aperture and the width is not well determined the similarity may be by chance.

The Stripa tracer experiments were also analysed for matrix diffusion effects and the "flow wetted surface" was estimated to vary between 0.2 and 2 possibly up to 20 $m^2/m^3$ for the different tracers. The flow wetted surface in the model grid is

$$a = \frac{6\,W}{Z^2} \tag{15}$$

It is 0.4 for Z=1.2 and 0.2 $m^2/m^3$ for Z=1.7 m. The values fall within the range measured in the actual field experiment but the uncertainties are to large at present to draw any firm conclusions.

# 6 DISCUSSION AND CONCLUSIONS

The model proposed is intentionally made simple so that it is easy to incorporate tracer transport and to accommodate interacting tracers. The model must be calibrated to field measurements. Borehole transmissity data obtained by "narrow packer intervals should in principle suffice to obtain the effective channel lengths provided channel widths can be determined independently. The comparisons and calibrations with field observations are rather straightforward and have shown that the model can exhibit the properties of channeling observed in the field and that tracer residence time distributions and patterns also agree.

The good agreement between predicted flow porosity and flow wetted surface which was found in the Stripa experiments cannot by itself be used as a basis for model acceptance. Although encouraging, more comparisons with field tracer test are needed.

# 7 NOTATION

| | | |
|---|---|---|
| a | Wetted surface | $m^2/m^3$ |
| $b_o$ | Mean logarithm in aperture | |
| C | Conductance | |
| $D_{bh}$ | Hole diameter | L |
| L | Length | L |
| P | Pressure | $M/LT^2$ |
| Pe | Peclet number | |
| Q | Water flowrate | $L^3/T$ |
| W | Channel width | L |
| r | Radial distance | L |
| $t_w$ | Water residence time | T |
| Z | Channel length | L |
| | | |
| $\alpha$ | Angle | |
| $\delta$ | Aperture | L |
| $\varepsilon$ | Porosity | |
| $\lambda$ | Correlation length | L |
| $\mu$ | Dynamic viscosity | M/LT |
| $\sigma$ | Standard deviation in the lognormal distribution | |
| $\sigma_t$ | Standard deviation in the breakthrough curve | T |

# 8 REFERENCES

Abelin H. Migration in a single fracture. An in situ experiment in a natural fracture, Ph. D. Thesis, Dep. Chemical Engineering, Royal Institute of Technology, Stockholm, Sweden 1986

Abelin H., Neretnieks I., Tunbrant S., Moreno L. Final Report of the Migration in a Single Fracture - Experimental Results and Evaluation, Stripa Project Report 85-03, OECD/NEA, SKB 1985

Abelin H., Birgersson L., Gidlund J., Moreno L., Neretnieks I., Widén H., Ågren T, 3-D migration experiment - Report 3, Part I, Performed experiments, Results and Evaluation, Stripa Project Technical Report 87-21, Stockholm Nov. 1987

Abelin H., Birgersson L., Neretnieks I., Ågren T. A channeling experiment to study flow and transport in natural fractures, In Scientific Basis for Nuclear Waste Management XII, Berlin Nov 1988, Proceedings, p 661-668, 1989

Ahlbom K., Smellie J.A.T. Characterization of fracture zone 2, Finnsjön study-site, SKB TR 89-12, 1989

Black J., Holmes D., Brightman M. Cross hole investigations - Hydrological results and interpretations, Stripa project report 87-17 OECD/NEA, SKB Nov 1987

Cacas M.C., de Marsily G., Tillie B., Barbreau A., Durand E., Feuga B., Peaudecerf P. Modelling fracture flow with a stochastic discrete fracture network: calibration and validation - 1 The flow model, Water Resources Res., 26, p 479-489, 1990a

Cacas M.C., Ledoux E., de Marsily G., Barbreau A., Calmels P., Gaillard B., Margritta R. Modelling fracture flow with a stochastic discrete fracture network: calibration and validation - 2 The transport model, Water Resources Res., 26, p491-500, 1990b

Dverstorp B. Analyzing flow and transport in fractured rock using the discrete fracture network concept. Ph.D. Thesis Royal Institute of Technology, Dep. Hydraulic Engineering TRITA-VBI-151 Stockholm 1991

Geir J., Dershowitz W., Sharp G. Prediction of inflow into the D-holes in the Stripa mine. Stripa Project Technical Report 90-06. OECD/NEA, SKB April 1990

Herbert A and Splawski, B., Prediction of inflow into the D-holes at the Stripa mine, Stripa Project Technical Report 90-14. OECD/NEA, SKB, 1990

Holmes D., Abbot M., Brightman M. Site characterization and validation- Single borehole hydraulic testing of "C" boreholes, simulated drift experiments and small scale hydraulic testing, Stage 3. Stripa Project Technical Report 90-10. OECD/NEA, SKB April 1990

KBS-3, 1983, Final storage of spent nuclear fuel, Report by Swedish Nuclear Fuel Supply Co, SKBF, Stockholm, Sweden, May, 1983

Levenspiel, O., Chemical Reaction Engineering, 2nd ed., p 275. John Wiley, New York, 1972.

Long J.C.S., Endo H.K., Karasaki K., Pyrak L., MacLean P., Witherspoon P.A. Hydrological Behavior of Fracture Networks. Hydrogeology of Rocks of Low Permeability, IAH Conference Jan 7-12, 1985, Tucson Arizona. Volume XVII, p 44-468, 1985

Moreno L., Neretnieks I., Klockars C-E. Evaluation of some tracer tests in the granitic rock at Finnsjön, KBS TR 83-38, 1983

Moreno L., Tsang Y.W., Tsang C.F., Neretnieks I. Flow and solute transport in a single fracture. A two-dimensional statistical model, Nuclear Fuel Safety Project, Technical report TR 88-03, Stockholm, 1987

Moreno L., Tsang Y.W., Tsang C.F., Hale F.V., Neretnieks I. Flow and tracer transport in a single fracture. A stochastic model and its relation to some field observations, Water Resources Research, 24, p 2033-3048, 1988

Moreno L., Neretnieks I., Landström O. An evaluation of some tracer tests performed at Studsvik, KBS TR 89-09, 1989

NAGRA Project Gewähr. Endlager Für Hochaktive Abfälle: Das System der Sicherheitsbarriären, Nagra, Baden, Switzerland, Jan 1985

Neretnieks I. Diffusion in the Rock Matrix: An Important Factor in Radionuclide Retardation? J. Geophys. Res. 85, p 4379-4397, 1980

Neretnieks I. Channeling in crystalline rocks. Its possible impact on transport of radionuclides from a repository, Colloque international Impact de la physico-chimie sur l'étude, la conception et l'optimisation des procédes en milieu poreux naturel, Nancy, 10-12 Juin 1987a

Neretnieks I. Channeling effects in flow and transport in fractured rocks - Some recent observations and models, Paper presented at GEOVAL symposium, Stockholm, Proceedings, p 315-335, 1987b

Neretnieks I., Abelin H., Birgersson L. Some recent observations of channeling in fractured rocks. Its potential impact on radionuclide migration, In DOE/AECL conference Sept 15-17, 1987, San Francisco, Proceedings p 387-410, 1987

Palmqvist K. Kymmens kraftverk. Fullortsborrad tunnel. Hydrogeologisk kartering och utvärdering. Report Bergab AB company. Göteborg 1987

Palmqvist K., Lindström M. Channel widths. SKB Arbetsrapport 91-06. February 1991

Robinson P.C., Connectivity, flow and and transport in network models of fractured media, Ph. D. Thesis, St. Catherine's College, Oxford University, Ref TP 1072, May 1984

Smith L., Schwartz F., Mase C. Applications of stochastic methods for the simulation of solute transport in discrete and continuum models of fractured rock systems, Proceedings of Conference on Geostatistical, Sensitivity and Uncertainty Methods for Ground-Water Flow and Radionuclide Transport Modelling, San Francisco, California, September 15-17, p 425-440, 1987

Tsang Y.W., Tsang C.F., Neretnieks I., Moreno L. Flow and tracer transport in fractured media - A variable aperture channel model and its properties, Water Resources Research 24, p 2049-2060, 1988

Witherspoon P.A., Wang J.S.K., Iwai K., Gale J.E. Validity of cubic law for fluid flow in a deformable rock fracture, Water Resources Res. 16, p 1016-1024, 1980.

Tamashita R., Kimura H., Particle-tracking technique for nuclide decay chain transport in fractured porous media, Journal of Nuclear Science and Technology, 27, p 1041-1049, 1990.

KBS - technical reports can be obtained from: INIS CLEARING HOUSE, International Atomic Energy Agency, P.O. Box 100, A-1400 VIENNA, Austria.

# *List of SKB reports*

## Annual Reports

*1977-78*
TR 121
**KBS Technical Reports 1 – 120**
Summaries
Stockholm, May 1979

*1979*
TR 79-28
**The KBS Annual Report 1979**
KBS Technical Reports 79-01 – 79-27
Summaries
Stockholm, March 1980

*1980*
TR 80-26
**The KBS Annual Report 1980**
KBS Technical Reports 80-01 – 80-25
Summaries
Stockholm, March 1981

*1981*
TR 81-17
**The KBS Annual Report 1981**
KBS Technical Reports 81-01 – 81-16
Summaries
Stockholm, April 1982

*1982*
TR 82-28
**The KBS Annual Report 1982**
KBS Technical Reports 82-01 – 82-27
Summaries
Stockholm, July 1983

*1983*
TR 83-77
**The KBS Annual Report 1983**
KBS Technical Reports 83-01 – 83-76
Summaries
Stockholm, June 1984

*1984*
TR 85-01
**Annual Research and Development Report 1984**
Including Summaries of Technical Reports Issued during 1984. (Technical Reports 84-01 – 84-19)
Stockholm, June 1985

*1985*
TR 85-20
**Annual Research and Development Report 1985**
Including Summaries of Technical Reports Issued during 1985. (Technical Reports 85-01 – 85-19)
Stockholm, May 1986

*1986*
TR 86-31
**SKB Annual Report 1986**
Including Summaries of Technical Reports Issued during 1986
Stockholm, May 1987

*1987*
TR 87-33
**SKB Annual Report 1987**
Including Summaries of Technical Reports Issued during 1987
Stockholm, May 1988

*1988*
TR 88-32
**SKB Annual Report 1988**
Including Summaries of Technical Reports Issued during 1988
Stockholm, May 1989

*1989*
TR 89-40
**SKB Annual Report 1989**
Including Summaries of Technical Reports Issued during 1989
Stockholm, May 1990

*1990*
TR 90-46
**SKB Annual Report 1990**
Including Summaries of Technical Reports Issued during 1990
Stockholm, May 1991

## Technical Reports

### List of SKB Technical Reports 1991

TR 91-01
**Description of geological data in SKB's database GEOTAB**
**Version 2**
Stefan Sehlstedt, Tomas Stark
SGAB, Luleå
January 1991

TR 91-02
**Description of geophysical data in SKB database GEOTAB**
**Version 2**
Stefan Sehlstedt
SGAB, Luleå
January 1991

TR 91-03
**1. The application of PIE techniques to the study of the corrosion of spent oxide fuel in deep-rock ground waters**
**2. Spent fuel degradation**
R S Forsyth
Studsvik Nuclear
January 1991

TR 91-04
**Plutonium solubilities**
I Puigdomènech[1], J Bruno[2]
[1]Enviromental Services, Studsvik Nuclear, Nyköping, Sweden
[2]MBT Tecnologia Ambiental, CENT, Cerdanyola, Spain
February 1991

TR 91-05
**Description of tracer data in the SKB database GEOTAB**
SGAB, Luleå
April, 1991

TR 91-06
**Description of background data in the SKB database GEOTAB**
**Version 2**
Ebbe Eriksson, Stefan Sehlstedt
SGAB, Luleå
March 1991

TR 91-07
**Description of hydrogeological data in the SKB's database GEOTAB**
**Version 2**
Margareta Gerlach[1], Bengt Gentzschein[2]
[1]SGAB, Luleå
[2]SGAB, Uppsala
April 1991

TR 91-08
**Overview of geologic and geohydrologic conditions at the Finnsjön site and its surroundings**
Kaj Ahlbom[1], Sven Tirén[2]
[1]Conterra AB
[2]Sveriges Geologiska AB
January 1991

TR 91-09
**Long term sampling and measuring program. Joint report for 1987, 1988 and 1989. Within the project: Fallout studies in the Gideå and Finnsjö areas after the Chernobyl accident in 1986**
Thomas Ittner
SGAB, Uppsala
December 1990

TR 91-10
**Sealing of rock joints by induced calcite precipitation. A case study from Bergeforsen hydro power plant**
Eva Hakami[1], Anders Ekstav[2], Ulf Qvarfort[2]
[1]Vattenfall HydroPower AB
[2]Golder Geosystem AB
January 1991

TR 91-11
**Impact from the disturbed zone on nuclide migration – a radioactive waste repository study**
Akke Bengtsson[1], Bertil Grundfelt[1], Anders Markström[1], Anders Rasmuson[2]
[1]KEMAKTA Konsult AB
[2]Chalmers Institute of Technology
January 1991

TR 91-12
**Numerical groundwater flow calculations at the Finnsjön site**
Björn Lindbom, Anders Boghammar, Hans Lindberg, Jan Bjelkås
KEMAKTA Consultants Co, Stockholm
February 1991

TR 91-13
**Discrete fracture modelling of the Finnsjön rock mass**
**Phase 1 feasibility study**
J E Geier, C-L Axelsson
Golder Geosystem AB, Uppsala
March 1991

TR 91-14
**Channel widths**
Kai Palmqvist, Marianne Lindström
BERGAB-Berggeologiska Undersökningar AB
February 1991

TR 91-15
**Uraninite alteration in an oxidizing environment and its relevance to the disposal of spent nuclear fuel**
Robert Finch, Rodney Ewing
Department of Geology, University of New Mexico
December 1990

TR 91-16
**Porosity, sorption and diffusivity data compiled for the SKB 91 study**
Fredrik Brandberg, Kristina Skagius
Kemakta Consultants Co, Stockholm
April 1991

TR 91-17
**Seismically deformed sediments in the Lansjärv area, Northern Sweden**
Robert Lagerbäck
May 1991

TR 91-18
**Numerical inversion of Laplace transforms using integration and convergence acceleration**
Sven-Åke Gustafson
Rogaland University, Stavanger, Norway
May 1991

TR 91-19
**NEAR21 - A near field radionuclide migration code for use with the PROPER package**
Sven Norman[1], Nils Kjellbert[2]
[1]Starprog AB
[2]SKB AB
April 1991

TR 91-20
**Äspö Hard Rock Laboratory. Overview of the investigations 1986-1990**
R Stanfors, M Erlström, I Markström
June 1991

TR 91-21
**Äspö Hard Rock Laboratory. Field investigation methodology and instruments used in the pre-investigation phase, 1986-1990**
K-E Almén, O Zellman
June 1991

TR 91-22
**Äspö Hard Rock Laboratory. Evaluation and conceptual modelling based on the pre-investigations 1986-1990**
P Wikberg, G Gustafson, I Rhén, R Stanfors
June 1991

TR 91-23
**Äspö Hard Rock Laboratory. Predictions prior to excavation and the process of their validation**
Gunnar Gustafson, Magnus Liedholm, Ingvar Rhén, Roy Stanfors, Peter Wikberg
June 1991

TR 91-24
**Hydrogeological conditions in the Finnsjön area. Compilation of data and conceptual model**
Jan-Erik Andersson, Rune Nordqvist, Göran Nyberg, John Smellie, Sven Tirén
February 1991

TR 91-25
**The role of the disturbed rock zone in radioactive waste repository safety and performance assessment. A topical discussion and international overview.**
Anders Winberg
June 1991

TR 91-26
**Testing of parameter averaging techniques for far-field migration calculations using FARF31 with varying velocity.**
Akke Bengtsson[1], Anders Boghammar[1], Bertil Grundfelt[1], Anders Rasmuson[2]
[1]KEMAKTA Consultants Co
[2]Chalmers Institute of Technology

TR 91-27
**Verification of HYDRASTAR. A code for stochastic continuum simulation of groundwater flow**
Sven Norman
Starprog AB
July 1991

TR 91-28
**Radionuclide content in surface and groundwater transformed into breakthrough curves. A Chernobyl fallout study in an forested area in Northern Sweden**
Thomas Ittner, Erik Gustafsson, Rune Nordqvist
SGAB, Uppsala
June 1991

TR 91-29
**Soil map, area and volume calculations in Orrmyrberget catchment basin at Gideå, Northern Sweden**
Thomas Ittner, P-T Tammela, Erik Gustafsson
SGAB, Uppsala
June 1991

TR 91-30
**A resistance network model for radionuclide transport into the near field surrounding a repository for nuclear waste (SKB, Near Field Model 91)**
Lennart Nilsson, Luis Moreno, Ivars Neretnieks, Leonardo Romero
Department of Chemical Engineering,
Royal Institute of Technology, Stockholm
June 1991

TR 91-31
**Near field studies within the SKB 91 project**
Hans Widén, Akke Bengtsson, Bertil Grundfelt
Kemakta Consultants AB, Stockholm
June 1991

TR 91-32
**SKB/TVO Ice age scenario**
Kaj Ahlbom[1], Timo Äikäs[2], Lars O. Ericsson[3]
[1]Conterra AB
[2]Teollisuuden Voima Oy (TVO)
[3]Svensk Kärnbränslehantering AB (SKB)
June 1991

TR 91-33
**Transient nuclide release through the bentonite barrier - SKB 91**
Akke Bengtsson, Hans Widén
Kemakta Konsult AB
May 1991

TR 91-34
**SIMFUEL dissolution studies in granitic groundwater**
I Casas[1], A Sandino[2], M S Caceci[1], J Bruno[1], K Ollila[3]
[1]MBT Tecnologia Ambiental, CENT, Cerdanyola, Spain
[2]KTH, Dpt. of Inorganic Chemistry, Stockholm, Sweden
[3]VTT, Tech. Res. Center of Finland, Espoo, Finland
September 1991

TR 91-35
**Storage of nuclear waste in long boreholes**
Håkan Sandstedt[1], Curt Wichmann[1], Roland Pusch[2], Lennart Börgesson[2], Bengt Lönnerberg[3]
[1]Tyréns
[2]Clay Technology AB
[3]ABB Atom
August 1991

TR 91-36
**Tentative outline and siting of a repository for spent nuclear fuel at the Finnsjön site. SKB 91 reference concept**
Lars Ageskog, Kjell Sjödin
VBB VIAK
September 1991

TR 91-37
**Creep of OFHC and silver copper at simulated final repository canister-service conditions**
Pertti Auerkari, Heikki Leinonen, Stefan Sandlin
VTT, Metals Laboratory, Finland
September 1991

TR 91-38
**Production methods and costs of oxygen free copper canisters for nuclear waste disposal**
Hannu Rajainmäki, Mikko Nieminen, Lenni Laakso
Outokumpu Poricopper Oy, Finland
June 1991

TR 91-39
**The reducibility of sulphuric acid and sulphate in aqueous solution (translated from German)**
Rolf Grauer
Paul Scherrer Institute, Switzerland
July 1990

TR 91-40
**Interaction between geosphere and biosphere in lake sediments**
Björn Sundblad, Ignasi Puigdomenech, Lena Mathiasson
December 1990

TR 91-41
**Individual doses from radionuclides released to the Baltic coast**
Ulla Bergström, Sture Nordlinder
Studsvik AB
May 1991

TR 91-42
**Sensitivity analysis of the groundwater flow at the Finnsjön study site**
Yung-Bing Bao, Roger Thunvik
Dept. Land and Water Resources,
Royal Institute of Technology, Stockholm, Sweden
September 1991

TR 91-43

**SKB - PNC**

# Development of tunnel radar antennas

Lars Falk
ABEM, Uppsala, Sweden

July 1991